

Dopaminergic Transmission Rapidly and Persistently Enhances Excitability of D1 Receptor-Expressing Striatal Projection Neurons

Highlights

- Phasic dopamine release elevates D1-SPN firing for minutes with subsecond onset
- Excitability is enhanced both in the up state and in transition from the down state
- Modulation may involve dynamic effects on voltage- and Ca^{2+} -dependent K^+ channels
- Minimally invasive recording is required to preserve native dopaminergic modulation

Authors

Asha K. Lahiri, Mark D. Bevan

Correspondence

m-bevan@northwestern.edu

In Brief

Lahiri and Bevan demonstrate that dopaminergic transmission powerfully enhances the intrinsic excitability of D1 receptor-expressing striatal projection neurons in a state-independent manner. Dynamic biophysical changes argue that different ion channel mechanisms may underlie the initial and long-lasting phases of modulation.



Dopaminergic Transmission Rapidly and Persistently Enhances Excitability of D1 Receptor-Expressing Striatal Projection Neurons

Asha K. Lahiri¹ and Mark D. Bevan^{1,2,*}

¹Department of Physiology, Feinberg School of Medicine, Northwestern University, Chicago, IL 60611, USA

²Lead Contact

*Correspondence: m-bevan@northwestern.edu

<https://doi.org/10.1016/j.neuron.2020.01.028>

SUMMARY

Substantia nigra dopamine neurons have been implicated in the initiation and invigoration of movement, presumably through their modulation of striatal projection neuron (SPN) activity. However, the impact of native dopaminergic transmission on SPN excitability has not been directly demonstrated. Using perforated patch-clamp recording, we found that optogenetic stimulation of nigrostriatal dopamine axons rapidly and persistently elevated the excitability of D1 receptor-expressing SPNs (D1-SPNs). The evoked firing of D1-SPNs increased within hundreds of milliseconds of stimulation and remained elevated for ≥ 10 min. Consistent with the negative modulation of depolarization- and Ca^{2+} -activated K^+ currents, dopaminergic transmission accelerated subthreshold depolarization in response to current injection, reduced the latency to fire, and transiently diminished action potential afterhyperpolarization. Persistent modulation was protein kinase A dependent and associated with a reduction in action potential threshold. Together, these data demonstrate that dopaminergic transmission potently increases D1-SPN excitability with a time course that could support subsecond and sustained behavioral control.

INTRODUCTION

Dopaminergic modulation of the dorsolateral striatum (DLS) has long been recognized as critical for movement. In idiopathic and experimental Parkinson's disease, progressive degeneration of DLS-projecting substantia nigra (SN) dopamine (DA) neurons leads to slowly emerging deficits in movement initiation and vigor (Mazzoni et al., 2007; Panigrahi et al., 2015). Furthermore, recent studies suggest that SN DA neurons also play a more dynamic role in movement control: (1) transient increases in their activity consistently precede movement initiation and/or acceleration; (2) optogenetic stimulation of their cell bodies or axon terminals in the dorsal striatum can trigger movement within hundreds of

milliseconds; and (3) brief optogenetic inhibition of their cell bodies impairs subsequent initiation of spontaneous or learned action sequences (Barter et al., 2015; Coddington and Dudman, 2018; da Silva et al., 2018; Howe and Dombek, 2016).

It is thought that SN DA neurons promote movement through their modulation of striatal projection neuron (SPN) excitability. Indeed, SPNs express either D1- or D2-class DA receptors whose activation can modify their sensitivity to motor commands. Furthermore, SPN activity is correlated with and causally linked to the initiation and execution of action sequences (Cui et al., 2013; Kravitz et al., 2010; Markowitz et al., 2018; Tecuapetla et al., 2016). The majority of D1 receptor-expressing SPNs (D1-SPNs) project to basal ganglia output nuclei, forming the so-called direct pathway, which is thought to promote selected actions (Cui et al., 2013; Kravitz et al., 2010). D2 receptor-expressing SPNs (D2-SPNs) instead give rise to the indirect pathway, which is posited to inhibit competing movements, thus permitting selected actions to proceed unencumbered (Cui et al., 2013; Freeze et al., 2013; Mink, 1996).

Recent studies have shown that optogenetic stimulation of either nigrostriatal DA axons or D1-SPNs rapidly triggers ambulation (Howe and Dombek, 2016; Roseberry et al., 2016). While it is plausible that nigrostriatal DA release contributes to locomotion-related D1-SPN activity, precisely how—and how quickly—native transmission regulates D1-SPN firing remains unknown. The effects of D1-like receptor (D1R) activation have traditionally been investigated using exogenous DA or D1R agonists in conjunction with whole-cell patch-clamp recording *ex vivo*. This approach has provided fundamental insight into D1R signaling mechanisms and its molecular targets. D1Rs couple to $\text{G}\alpha_{s/o/f}$ proteins, which, through their stimulation of adenylyl cyclase, elevate cyclic adenosine monophosphate (cAMP) levels and activate protein kinase A (PKA) (Gerfen and Surmeier, 2011). This canonical signaling pathway modulates a variety of intracellular targets, including ion channels that regulate D1-SPN excitability (Beaulieu and Gainetdinov, 2011; Greengard, 2001). However, traditional experimental approaches have generated contradictory data concerning the effects of D1R signaling on excitability at both hyperpolarized "down-state" and depolarized "up-state" membrane potentials (Gerfen and Surmeier, 2011). In addition, the sustained application of D1R agonists at high concentrations does not mimic the spatiotemporal profile of endogenous DA release (Patriarchi et al., 2018; Sulzer et al., 2016) and is likely to promote receptor desensitization (Fiorillo



and Williams, 1998; Gainetdinov et al., 2004). The use of whole-cell patch-clamp recording is also problematic, because G protein-coupled receptor (GPCR) signaling cascades rely on second messengers that are sensitive to dialysis (Horn and Marty, 1988). Perhaps as a result of these issues, a recent computational analysis found that published mechanisms of dopaminergic signaling in D1-SPNs were too slow to account for subsecond behavioral control (Lindroos et al., 2018). To determine whether more rapid modulation of excitability could be revealed, we utilized brief optogenetic stimulation of nigrostriatal DA axons in conjunction with gramicidin-based perforated patch-clamp recording (Kyrozis and Reichling, 1995) of visually identified D1-SPNs *ex vivo*. This approach enabled us to measure the impact of intact D1R signaling, triggered by endogenous DA release, on the intrinsic excitability of D1-SPNs. We found that physiological patterns of nigrostriatal transmission powerfully enhanced D1-SPN excitability within hundreds of milliseconds, with effects lasting for at least 10 min, providing a potential mechanism for the rapid and sustained regulation of movement by DA.

RESULTS

Population data are presented as individual data points with superimposed box plots illustrating the median (central line), interquartile range (box), and 10%–90% range (whiskers) of each group. Paired data are indicated by line plots. Non-parametric statistical comparisons were made using the Wilcoxon signed-rank (WSR) test for paired data or the Mann-Whitney U (MWU) test for unpaired data. Associated p values have been corrected for multiple comparisons where appropriate (Holm, 1979; Tables S1–S10).

Nigrostriatal Dopaminergic Transmission Enhances the Evoked Firing of D1-SPNs

To assess the effects of dopaminergic transmission on D1-SPN excitability in the DLS, we combined optogenetic stimulation of nigrostriatal axons with perforated patch-clamp recording of identified D1-SPNs in *ex vivo* brain slices. Channelrhodopsin-2 (ChR2) was expressed in DA neurons through stereotaxic injection of an adeno-associated virus (AAV) carrying a Cre recombinase-dependent ChR2(H134R)-eYFP expression construct into the SN of adult $DAT^{RES-Cre/WT}$; $Drd1a$ -tdTomato $^{+/+}$ mice (Figure 1A). $DAT^{RES-Cre}$ mice express Cre recombinase under the transcriptional control of the DA transporter (DAT) promoter, enabling specific opsin expression in DA neurons (Bäckman et al., 2006; Figures 1B and 1C). $Drd1a$ -tdTomato mice exhibit tdTomato fluorescence in D1R-expressing neurons, facilitating their visual identification *ex vivo* (Ade et al., 2011; Figure 1C). Fast-scan cyclic voltammetry (FSCV) was first performed to determine striatal DA levels and dynamics following either single-pulse (2 ms) or pulse-train (5 pulses, 2 ms each) optogenetic stimulation of DA axons. Pulse-train frequencies were chosen to mimic the *in vivo* tonic (4 Hz) and phasic (20 Hz) firing patterns of midbrain DA neurons (Grace and Bunney, 1984a, 1984b; Marinelli and McCutcheon, 2014). Consistent with previous reports (Bass et al., 2013; Melchior et al., 2015), peak evoked DA concentrations scaled with increasing stimulus frequency and de-

cayed to baseline levels in < 5 s (Figures 1D–1F and S1A–S1C). Maximal evoked DA concentrations were largely sub-micromolar, similar to naturally occurring DA transients measured *in vivo* (Robinson et al., 2002).

We next examined the impact of optogenetically evoked DA on D1-SPN excitability. In addition to their expression of tdTomato, D1-SPNs were identified by their characteristic (1) somatic diameter of ~10–15 μ m; (2) hyperpolarized resting membrane potential, ~10–15 mV above the equilibrium potential for K^+ ($E_K = -100$ mV); and (3) slow depolarization and long latency to fire in response to rheobase current injection. Long (> 10 s) somatic current pulses were delivered to evoke D1-SPN firing (hereafter referred to as the “long up-state” protocol). Optogenetic stimulation was delivered after allowing firing to stabilize for 5 s, and current injection was maintained for an additional 5 s so that steady-state firing rates could be compared before and after DA release. To isolate the direct effects of dopaminergic transmission on D1-SPNs, recordings were made in the presence of GABA_A, GABA_B, NMDA, AMPA/kainate, and nicotinic and muscarinic acetylcholine receptor antagonists. Single-pulse, 4 Hz, and 20 Hz optogenetic stimulation each robustly increased the frequency of evoked firing (Figures 1G, 1H, S1D, and S1E). Because intrinsic properties like spike-frequency adaptation can prevent D1-SPNs from reaching a steady-state level of activity, it was useful to compare evoked firing with and without optogenetic stimulation. In this way, dopaminergic modulation of firing could be disambiguated from changes due to prolonged depolarization: adjusted effect of DA = (post-stimulus frequency – pre-stimulus frequency) – (late current frequency – early current frequency), where early and late current time points on current-only trials corresponded to pre- and post-stimulus time points on optogenetic stimulation trials (Figures S1G and S1H). Compared to current injection alone, optogenetic stimulation of DA axons (either single-pulse or pulse-train stimulation at 4 Hz or 20 Hz) elevated D1-SPN firing frequency substantially and to a similar degree (Figures 1I and S1F). Because optogenetic stimulation simultaneously activates many axons, it is better suited to mimic synchronous, phasic DA neuron activity rather than tonic, asynchronous activity. Therefore, subsequent optogenetic stimulation was delivered at 20 Hz. Optogenetically evoked acceleration of D1-SPN firing was no longer observed following bath application of the D1R antagonist SCH 23390 (0.5 μ M), confirming its dependence on D1R activation (Figures 1J–1L).

Dopaminergic Transmission Rapidly Triggers Long-Lasting, PKA-Dependent Elevation of D1-SPN Firing

To determine the onset kinetics of dopaminergic modulation, we set a threshold of 3 standard deviations (SDs) above the mean instantaneous firing rate in the 2 s immediately preceding optogenetic stimulation. Modulation onset was defined as the first time that instantaneous firing frequency exceeded this threshold for two consecutive interspike intervals. 35 of 38 neurons exhibited modulation according to this measure, 33 of which were modulated within 1 s (median onset = 458.1 ms; Figures 2A–2C). Following modulation onset, firing frequency remained elevated for the duration of the current step (Figure 2D). Indeed, D1-SPN excitability was persistently elevated for at least 10 min

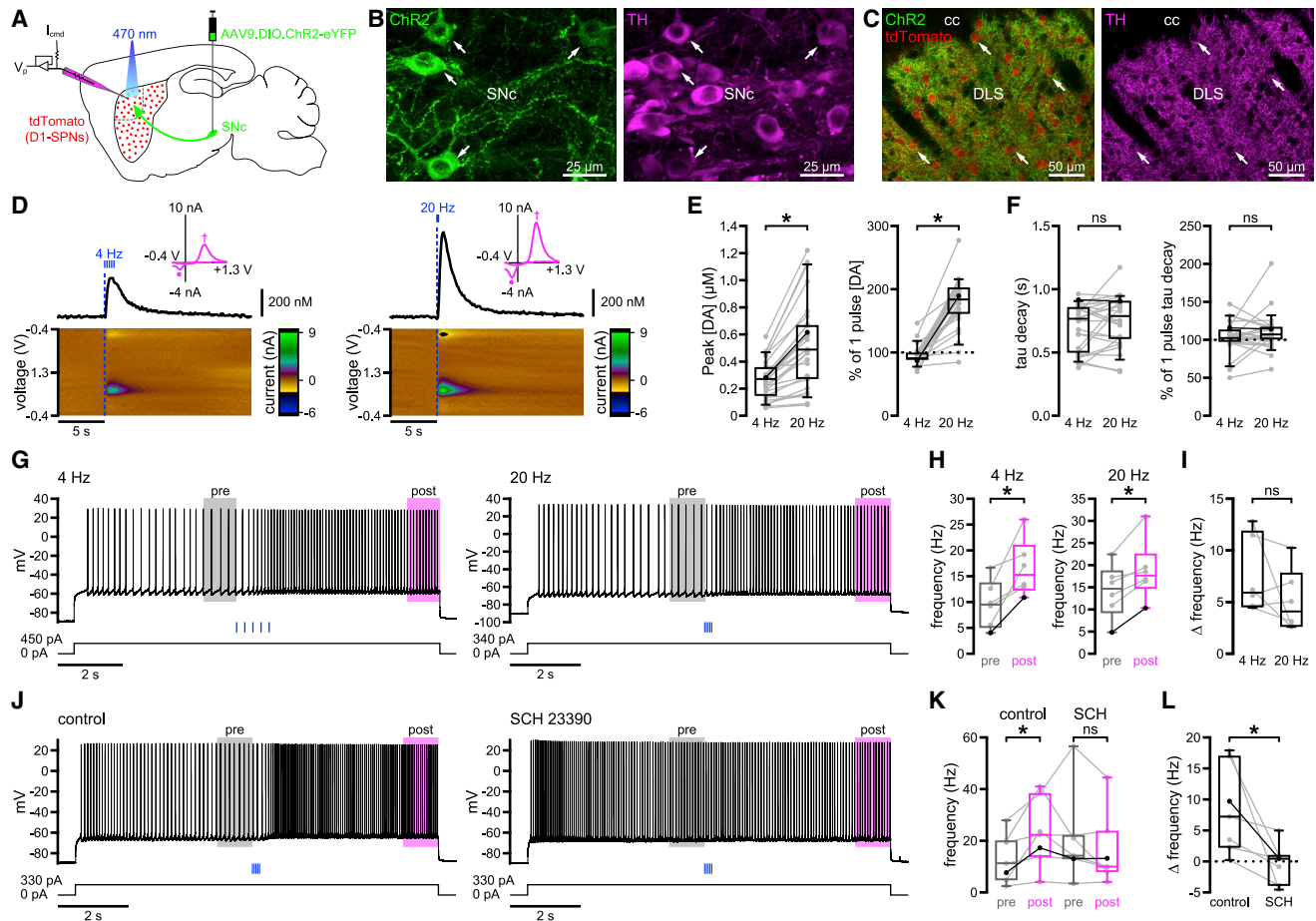


Figure 1. Optogenetic Stimulation of Nigrostriatal DA Axons Elevates the Frequency of Evoked Firing in D1-SPNs

(A) Schematic of the experimental approach.

(B) Viral expression of ChR2(H134R)-eYFP (green) in tyrosine hydroxylase (TH)-immunoreactive (magenta) SN pars compacta (SNc) DA neurons (arrows).

(C) Viral expression of ChR2(H134R)-eYFP (green) in TH-immunoreactive (magenta) DA axons in the vicinity of tdTomato-expressing D1-SPNs (red; arrows) in the DLS (cc, corpus callosum).

(D–F) Optogenetically evoked (blue) DA transients reached maximal levels that scaled with stimulus frequency and decayed within seconds (D, example FSCV signals; E and F, population data with bold lines indicating examples in D). Magenta insets in (D) show cyclic voltammograms indicating peak oxidation (\uparrow , 0.6 V) and reduction (\downarrow , -0.2 V) potentials for DA.

(G–I) The current-evoked firing of D1-SPNs was elevated following both 4 Hz and 20 Hz optogenetic stimulation (blue) of DA axons (G, examples; H and I, population data; H, bold lines indicate examples in G).

(J–L) Optogenetic stimulation of DA axons did not elevate firing in the presence of the D1R antagonist SCH 23390 (0.5 μ M) (J, example; K and L, population data with bold lines indicating example in J). Population data in (I) and (L) represent an adjusted measure of dopaminergic modulation relative to current injection alone. * $p < 0.05$; ns, not significant.

See also Figure S1 and Table S1.

following a single bout of optogenetic stimulation, as assessed by responses to 1 s current steps delivered once per minute for 3–4 min before (baseline) and 10–20 min after (post-stimulation) the long up-state protocol (Figures 2E, 2F, S2A, and S2B). Persistent modulation on the order of minutes may indicate the involvement of PKA-mediated protein phosphorylation (Gervasi et al., 2007; Ma et al., 2018). To test this possibility, we bath-applied a cell-permeable peptide inhibitor of PKA—PKI 14-22 amide, myristoylated (PKI, 1 μ M)—for at least 10 min prior to optogenetic stimulation and repeated our assay of persistent modulation. In the presence of PKI, post-stimulation firing rates remained unchanged from baseline levels (Figures 2G, 2H, S2C,

and S2D). This could not be attributed to direct, PKI-mediated effects on D1-SPN excitability, as neither baseline firing rates nor injected current amplitudes differed between control and PKI groups (Figure S2E; Table S2). Together, these findings suggest that dopaminergic transmission elicits long-lasting positive modulation of D1-SPN excitability that requires intact PKA signaling.

Dopaminergic Modulation of D1-SPN Excitability Is Disrupted in the Whole-Cell Configuration

In contrast to perforated-patch recordings, whole-cell recordings revealed little to no dopaminergic modulation of D1-SPN firing (Figures 3A–3C and S3A). Several whole-cell recording studies

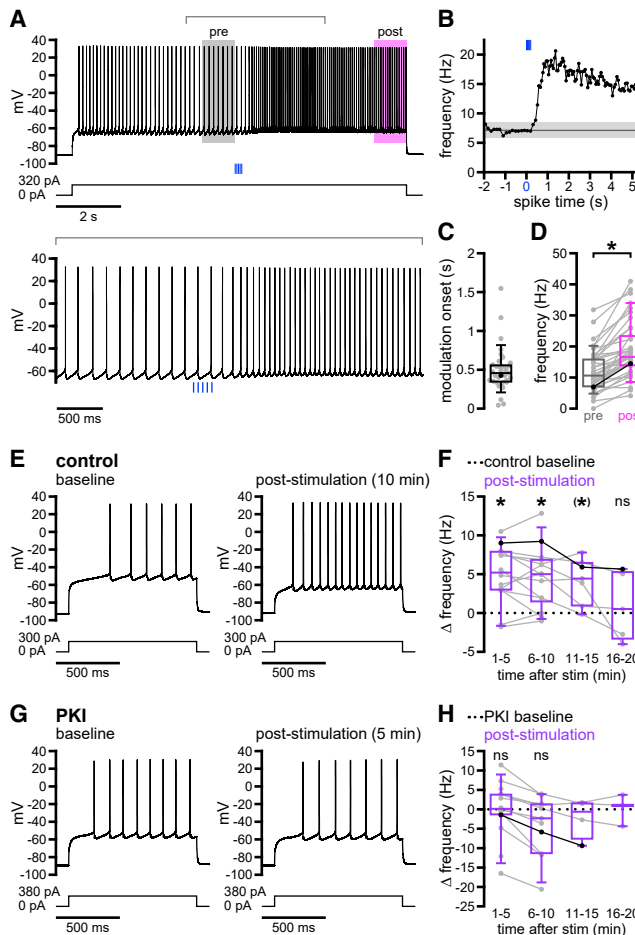


Figure 2. Dopaminergic Transmission Rapidly and Persistently Augments D1-SPN Firing

(A–D) Optogenetic stimulation (blue) of DA axons increased D1-SPN evoked firing with subsecond onset in the majority of neurons (A and B, example neuron; C and D, population data highlighting example shown in A and B). (B) Instantaneous frequencies for each interspike interval are shown relative to the start of stimulation, illustrating the method for determining modulation onset (dark gray, mean; light gray, ± 3 SDs). (C and D) Firing was rapidly enhanced (C) and remained elevated for the duration of the current step (D).

(E–H) DA release triggered a long-lasting increase in D1-SPN firing that required intact PKA signaling (E and G, examples; F and H, population data highlighting examples in E and G, respectively). (E and F) Evoked firing was enhanced relative to baseline for at least 10 min following a single bout of optogenetic stimulation. (G and H) Persistent modulation was not observed in the presence of the PKA inhibitor PKI 14-22 amide, myristoylated ($1 \mu\text{M}$). Statistical tests in (F) and (H) represent comparisons of absolute frequencies shown in Figures S2B and S2D; associated p values have been corrected for multiple comparisons. (H) Statistical tests were not conducted on groups of fewer than 5 neurons.

* $p < 0.05$ before and after Holm-Bonferroni correction (if corrected); (**) $p < 0.05$ before, but not after, correction; ns, not significant. Highlighted examples are indicated by bold dots and connected lines superimposed on population data plots.

See also Figure S2 and Table S2.

have reported that midbrain DA neurons co-release glutamate and/or GABA in the DLS (Chuhma et al., 2017; Kim et al., 2015; Tritsch et al., 2012; Trudeau et al., 2014). Therefore, as a positive control for stimulation of dopaminergic fibers, these experiments were initially conducted in the absence of GABA and glutamate receptor antagonists. Under these conditions, fast synaptic responses were observed in both the whole-cell and perforated-patch configurations (Figures S3B and S3C). The majority of these responses were glutamatergic excitatory postsynaptic potentials (EPSPs; 20/22 neurons: 5/7 perforated, 15/15 whole cell; Figure S3B). GABAergic inhibitory postsynaptic potentials (IPSPs) were observed less frequently (2/22 neurons: 2/7 perforated, 0/15 whole cell; Figure S3C). The effects of glutamatergic and GABAergic co-transmission were transient and did not disrupt the strength or dynamics of concurrent dopaminergic modulation in the perforated-patch configuration (data not shown).

Following pharmacological blockade of amino acidergic transmission, optogenetic stimulation consistently elevated D1-SPN firing in perforated recordings only (Figures 3A–3C and S3A). Although population-level effects were absent in the whole-cell configuration, when modulation was observed in individual recordings, its onset was markedly delayed: subsecond modulation was seen in only 3 of 15 whole-cell recordings (Figure S3D). In addition, D1-SPNs recorded in the whole-cell configuration exhibited relatively large fluctuations in firing rate within current-only trials, suggesting that intrinsic firing dynamics were also perturbed (Figure 3C). Series resistances associated with the whole-cell and perforated-patch configurations were not different (Table S3). Presumably, the failure to detect robust modulation in whole-cell recordings was due to dialysis of cytosolic components critical for dopaminergic signaling and intrinsic firing properties. In order to preserve dopaminergic modulation of D1-SPN excitability, all subsequent experiments were carried out in the perforated-patch configuration.

Dopaminergic Transmission Facilitates D1-SPN Down-to Up-State Transitions

Several studies have argued that dopaminergic modulation decreases the excitability of D1-SPNs at down-state and sub-threshold membrane potentials, thereby impeding transitions to the up state (Calabresi et al., 1987; Nicola et al., 2000; Pacheco-Cano et al., 1996). This effect has been attributed to enhancement of inwardly rectifying K⁺ currents (Pacheco-Cano et al., 1996) and to reduction of voltage-dependent Na⁺ (Na_v) channel availability (Surmeier et al., 1992). It has been further suggested that D1R-mediated facilitation of evoked discharge is only revealed upon sustained depolarization, which inactivates prominent K⁺ conductances, such as the slowly inactivating A-type current (I_{AS}) (Hernández-López et al., 1997; Surmeier et al., 2007). Therefore, we assessed the impact of dopaminergic transmission on D1-SPNs undergoing down- to up-state transitions mimicking those exhibited during cortical slow-wave activity *in vivo* (Wilson, 1993; Wilson and Kawaguchi, 1996). This “short up-state” protocol consisted of 250 ms current steps delivered once per second for 41 s, with 20 steps occurring before and after optogenetic stimulation of DA afferents (20 Hz for 1 s). This protocol was then repeated every 5 min for 3–4 trials.

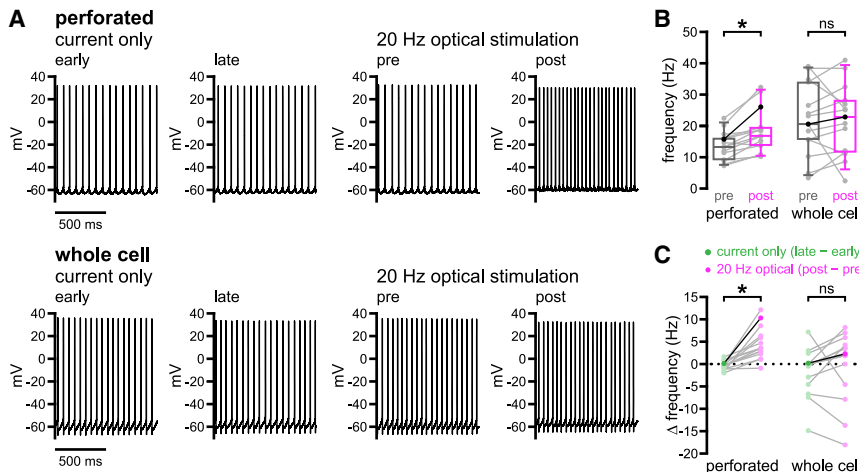


Figure 3. Optogenetic Stimulation of Dopaminergic Axons Does Not Positively Modulate the Evoked Firing of D1-SPNs Recorded in the Whole-Cell Configuration

(A–C) The evoked firing of D1-SPNs was elevated following 20 Hz optogenetic stimulation of DA axons when neurons were recorded in the perforated, but not the whole-cell, patch-clamp configuration (A, examples; B and C, population data with bold lines indicating examples in A).

* $p < 0.05$; ns, not significant.

See also Figure S3 and Table S3.

On the first trial, D1-SPN firing frequency increased and the latency to fire decreased substantially following optogenetic stimulation, suggesting that dopaminergic modulation promotes transitions from the down state to firing in the up state (Figures 4A–4C). While stimulation also elevated firing frequency and reduced spike latency on subsequent trials, the degree of pre-to post-stimulus modulation within each trial declined (Figures 4C–4E). The attenuation of acute modulation was accompanied by progressive shifts in pre-stimulus firing frequency and latency to fire (Figures 4C–4E). Together with the long-lasting modulation observed using the long up-state protocol (Figures 2E and 2F), these findings argue that the effects of dopaminergic modulation persisted between trials and may have contributed to the progressive occlusion of acute modulation. In order to test this idea, we bath-applied SCH 23390 (0.5 μ M) and continued to monitor D1-SPN responses to the short up-state protocol every 5 min. As expected, acute modulation of firing was eliminated in the presence of SCH 23390 (Figures 4F and 4G). Furthermore, pre-stimulus firing frequency and spike latency gradually returned to initial baseline levels after 20 min in the presence of SCH 23390 (Figures 4F and 4G), analogous to the slow decay of dopaminergic modulation observed using the long up-state protocol (Figures 2E and 2F). Together, these results suggest that nigrostriatal dopaminergic transmission promotes the activity of D1-SPNs undergoing down- to up-state transitions, accelerating both the onset of firing and the frequency of spike discharge thereafter. As for the modulation of firing during a prolonged up state, these effects were D1R-mediated and persisted for minutes following stimulation of DA release.

Biophysical Sequelae of Dopaminergic Modulation in D1-SPNs

DA may elevate D1-SPN excitability through its effects on multiple classes of ion channel. In the down state, SPN membrane potential is mainly determined by constitutively active, inwardly rectifying K^+ (Kir2) channels (Nisenbaum and Wilson, 1995; Shen et al., 2007). Activation of D1Rs by exogenous DA or D1R agonists has been linked to both enhancement (Pacheco-Cano et al., 1996; Zhao et al., 2016) and inhibition (Podda et al., 2010) of SPN Kir2 channels, which should either stabilize

the down state or promote up-state transitions. To examine the impact of dopaminergic transmission on D1-SPN Kir2 channels, a pair of sub- and suprathreshold current steps (250 ms each) was applied before and after optogenetic stimulation of nigrostriatal afferents (20 Hz for 250 ms) in the down state (Figure 5A). Subthreshold current amplitudes were chosen to elicit ~5–10 mV depolarization from rest in order to minimize the recruitment of other ion channels (Gabel and Nisenbaum, 1998; Nisenbaum et al., 1996; Nisenbaum and Wilson, 1995). Suprathreshold current steps were used as a positive control for dopaminergic modulation.

Since Kir2 channels are available at rest, their negative modulation should both depolarize the down state and increase the voltage response to subthreshold current injection. Positive modulation of Kir2 channels, on the other hand, may hyperpolarize or have no effect on resting membrane potential but should attenuate the depolarization generated by subthreshold current injection. Following optogenetic stimulation of nigrostriatal axons, D1-SPNs exhibited a consistent but tiny depolarization of resting membrane potential (Figures 5A and 5B). This effect was absent in the same neurons when membrane potential was measured at equivalent time points during current-only trials (Figure 5B). Optogenetic stimulation produced no change in either the voltage attained during subthreshold current injection or the amplitude of the associated depolarization (Figures 5A, 5C, and 5D). Together, these findings indicate neither appreciable negative nor positive modulation of Kir2 channels. In contrast, D1-SPN responses to suprathreshold current steps during the same trials revealed strong dopaminergic modulation of firing frequency and latency to fire (Figures 5E–5G).

Aside from Kir2, several other ion channels have been proposed as targets of D1R-dependent modulation. These include voltage-dependent K^+ (K_v) channels, such as $K_v1.2$ -containing channels underlying I_{AS} (Shen et al., 2004; Surmeier and Kitai, 1993); high-voltage-activated (HVA) Ca^{2+} channels, including L- (Ca_v1), P/Q- ($Ca_v2.1$), and N-type ($Ca_v2.2$) channels (Hernández-López et al., 1997; Surmeier et al., 1995); and Na_v1 channels (Surmeier et al., 1992). To further investigate the modulation of subthreshold conductances, we compared D1-SPN voltage trajectories during down- to up-state transitions before and after DA axon stimulation. Pre- and post-stimulus voltage responses to a 250 ms suprathreshold current step were superimposed,

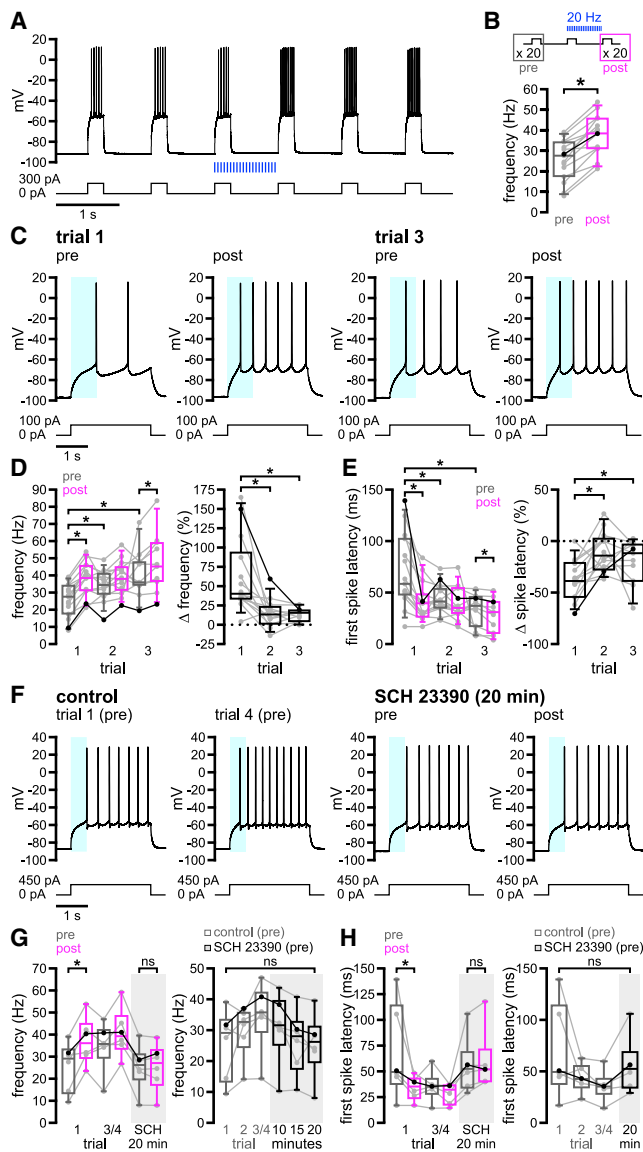


Figure 4. Nigrostriatal Dopaminergic Transmission Promotes D1-SPN Transitions from Rest in the Down State to Firing in the Up State

(A–E) Following 20 Hz optogenetic stimulation of DA axons (blue), the frequency and latency of D1-SPN firing evoked from down-state membrane potentials increased and decreased, respectively (A and C, examples; B, D, and E, population data; C, cyan highlight denotes the latency to fire prior to the first trial of optogenetic stimulation). (B) Schematic of the short up-state protocol (above); average firing frequency increased substantially following the first trial of optogenetic stimulation (below, with bold line indicating example in A). (D and E, with bold lines indicating example in C) The effects of optogenetic stimulation on firing persisted between trials conducted at 5-min intervals, leading to the progressive occlusion of acute—and accumulation of chronic—modulatory effects.

(F–H) Application of SCH 23390 (0.5 μM) led to inhibition of acute modulation and revealed gradual decay of prior modulation (F, example; G and H, population data with bold lines indicating example in F; F, cyan highlight denotes the latency to fire prior to stimulation in control trial 1).

* $p < 0.05$; ns, not significant.

See also Table S4.

aligned to the time of current onset, and then subtracted to identify the emergence of DA-sensitive components. These subtracted voltages were considered to reflect divergent pre- and post-stimulus trajectories when, for 3 consecutive samples, they exceeded the mean plus 3 SDs of voltage differences in the 20 ms preceding current injection (Figure 5H, right). According to this measure, differences in pre- and post-stimulus responses to current injection emerged rapidly and at subthreshold voltages (Figures 5H and 5I), consistent with the negative modulation of I_{AS} (Gabel and Nisenbaum, 1998; Nisenbaum et al., 1994). Dopaminergic modulation of the subthreshold voltage response was eliminated after application of SCH 23390 in 6 of 6 cells surveyed, indicating its dependence on D1R signaling (Figure 5H).

Enhancement of $Ca_{v}1$ channel currents has been proposed to underlie increased evoked discharge of SPNs following bath application of D1R agonists (Surmeier et al., 1995). $Ca_{v}1$ channels can generate a subthreshold conductance that augments firing, particularly during extended periods of depolarization (Hernández-López et al., 1997). We therefore tested whether bath application of isradipine, a negative allosteric modulator (NAM) of $Ca_{v}1$ channels, could reverse or prevent dopaminergic modulation of D1-SPN excitability during the long up-state protocol. In the presence of isradipine (5 μM), the increased firing in response to optogenetic stimulation of DA axons persisted (Figures S4A and S4B). Moreover, isradipine had no impact on the degree of modulation observed (Figure S4C). Isradipine (5–10 μM) also failed to prevent modulation in 4 of 4 D1-SPNs subjected to the short up-state protocol (Figures S4D and S4E). Together, these data argue that inhibition of $Ca_{v}1$ channels neither prevents nor attenuates dopaminergic modulation of D1-SPN firing induced by somatic depolarization and that $Ca_{v}1$ channel-independent mechanisms must be present.

D1R activation has also been proposed to reduce $Na_{v}1$ channel availability in SPNs (Surmeier et al., 1992), which should depolarize the threshold for action potentials and slow their rate of rise, thus limiting the elevation of firing. To examine the contribution of $Na_{v}1$ channel modulation, we compared action potentials before and after optogenetic stimulation during the long up-state protocol. Threshold values were determined from action potential waveform averages by detecting the first point of sustained positive acceleration (second derivative) of voltage, as described previously (Baufreton et al., 2005). Using this method, we observed no difference in threshold following nigrostriatal stimulation (Figures 6A and 6B). Other action potential properties, however, were subtly but significantly altered (Figures S5A–S5D). For example, the kinetics of the rising phase slowed modestly (Figure S5B). While this could indicate negative modulation of $Na_{v}1$ channels, it appears insufficient to oppose the elevation of firing.

Outward currents generated by K_v and Ca^{2+} -dependent K^+ channels are also thought to play an important role in regulating the frequency and pattern of D1-SPN activity. For example, (1) slowly inactivating $K_{v}1.2$ -containing channels limit the overall level of up-state depolarization and contribute to action potential afterhyperpolarization (AHP) (Nisenbaum et al., 1994; Shen et al., 2004), and (2) big- and small-conductance K^+ channels (BK and SK, respectively), through their selective coupling to Ca^{2+} entry

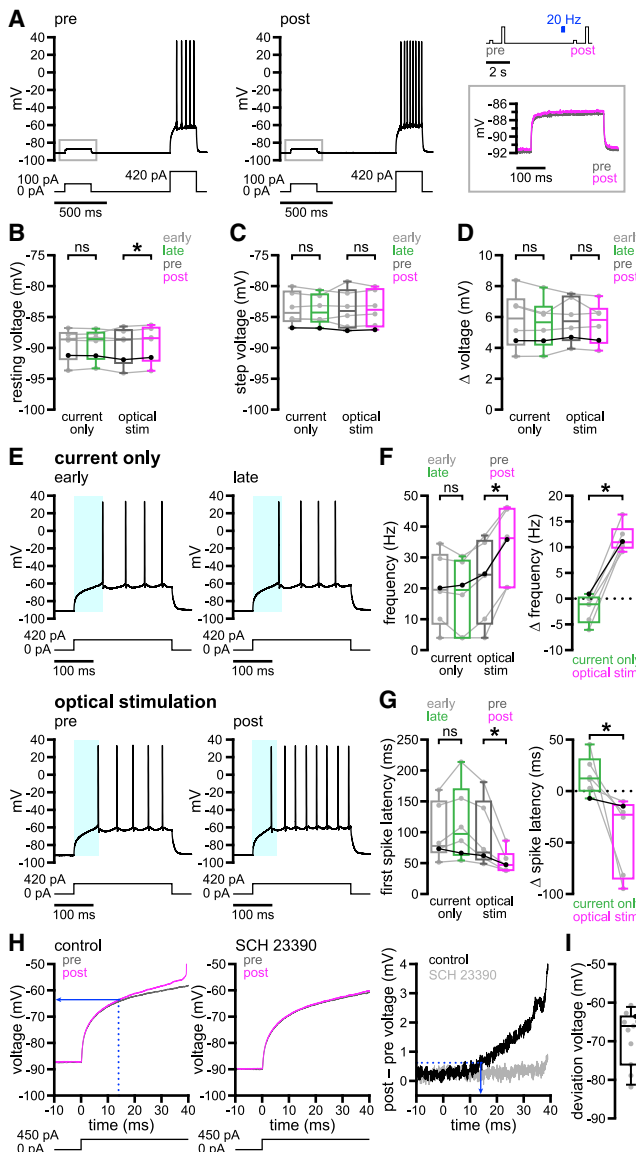


Figure 5. Dopaminergic Transmission Enhances D1-SPN Sub- and Suprathreshold Depolarization in a Manner Consistent with Modulation of I_{AS} but Not $Kir2$ Channels

(A–D) 20 Hz optogenetic stimulation of nigrostriatal DA axons (blue) had minimal effects on down-state resting membrane potential (B) and had no impact on the absolute voltage (C) or amplitude (D) of the response to current steps that generated < 10 mV depolarization (A, example with applied stimulation/current injection protocol and expanded subthreshold responses to the right; B–D, population data with bold lines indicating example in A).

(E–G) In contrast, optogenetic stimulation during the down state reduced the latency and increased the frequency of firing in response to suprathreshold current injection (E, example; F and G, population data with bold lines indicating example in E; E, cyan highlight denotes the latency to fire in early [above] or pre-stimulus [below] periods).

(H and I) Following dopaminergic transmission, responses to suprathreshold current injection were amplified at subthreshold voltages. (H, example; I, population data with bold dot indicating example in H). (H, left) Deviation voltage (blue, solid) was determined from the post-stimulus trace at the time of its divergence from the pre-stimulus trajectory (blue, dashed). (H, right) Time of

via $Ca_v2.1$ and $Ca_v2.2$ channels, contribute to the fast and medium-duration components of the AHP (fAHP and mAHP, respectively) (Pérez-Garcí et al., 2003; Pineda et al., 1992; Vilchis et al., 2000). Because D1R activation can reduce $K_v1.2$ -mediated currents as well as both $Ca_v2.1$ and $Ca_v2.2$ currents (Surmeier et al., 1995; Surmeier and Kitai, 1993), native dopaminergic modulation could potentially elevate firing through attenuation of the AHP and depolarization of the interspike interval. We therefore examined D1-SPN fAHP and mAHP peak voltages before and after optogenetic stimulation of DA axons. Using the long up-state protocol, AHPs were measured during the 2 s immediately preceding DA axon stimulation (pre-stimulus) and during the final 2 s of the current step (post-stimulus). We observed a reduction in both the fAHP and mAHP on optical-stimulation but not current-only trials (Figures 6C–6E and S5E). Analogous effects on all action potential properties were observed during the short up-state protocol (Figures S5F–S5M). To confirm that negative modulation of AHP components was dopaminergic in nature, we analyzed data from both short and long up-state protocols for a group of D1-SPNs recorded in the presence and absence of SCH 23390. Negative modulation of both the fAHP and mAHP was eliminated in the presence of SCH 23390 (Figures 6F–6H).

We next assessed whether persistent dopaminergic modulation of D1-SPN excitability was associated with the same biophysical changes described above. Using the assay of persistent modulation illustrated in Figure 2, we compared action potential properties at baseline with those measured 1 min after optogenetic stimulation. In contrast to its acute effects, persistent modulation was associated with a reduction in action potential threshold but no consistent change in AHP amplitudes (Figures 7A–7E). Furthermore, a positive correlation emerged between changes in threshold and changes in AHPs (Figure 7F), an effect that was not present immediately following stimulation (Figures S5E and S5M). While increased firing frequency and reduced latency to fire were consistent features of both acute and more persistent dopaminergic modulation, these results suggest that the underlying mechanisms are more dynamic than previously appreciated.

Negative modulation of $K_v1.2$ -containing, $Ca_v2.1$, and $Ca_v2.2$ channels may contribute to dopaminergic elevation of D1-SPN excitability. However, the perforated-patch recording configuration, while necessary to preserve dopaminergic modulation, is not suitable for direct examination of these currents under voltage clamp (see Discussion). We therefore examined whether the effects of DA on firing could be reproduced by application of α -dendrotoxin (α -DTX; 100 nM) to inhibit $K_v1.2$ -containing channels or apamin and iberiotoxin (Ap/IbTX; 100 nM each) to inhibit SK and BK channels, respectively. Dopaminergic elevation of firing frequency was mimicked by both α -DTX (Figures 8A and 8B) and Ap/IbTX (Figures 8D and 8E), although only α -DTX reduced spike latency (Figures 8C and 8F). Action potential threshold was not consistently altered in the presence of α -DTX (Figures 8G and

voltage deviation (blue, solid) was determined from the plot of voltage differences as described in Results (blue, dashed) and was not apparent in the presence of SCH 23390 (0.5 μ M).

* p < 0.05; ns, not significant.

See also Figure S4 and Tables S5 and S6.

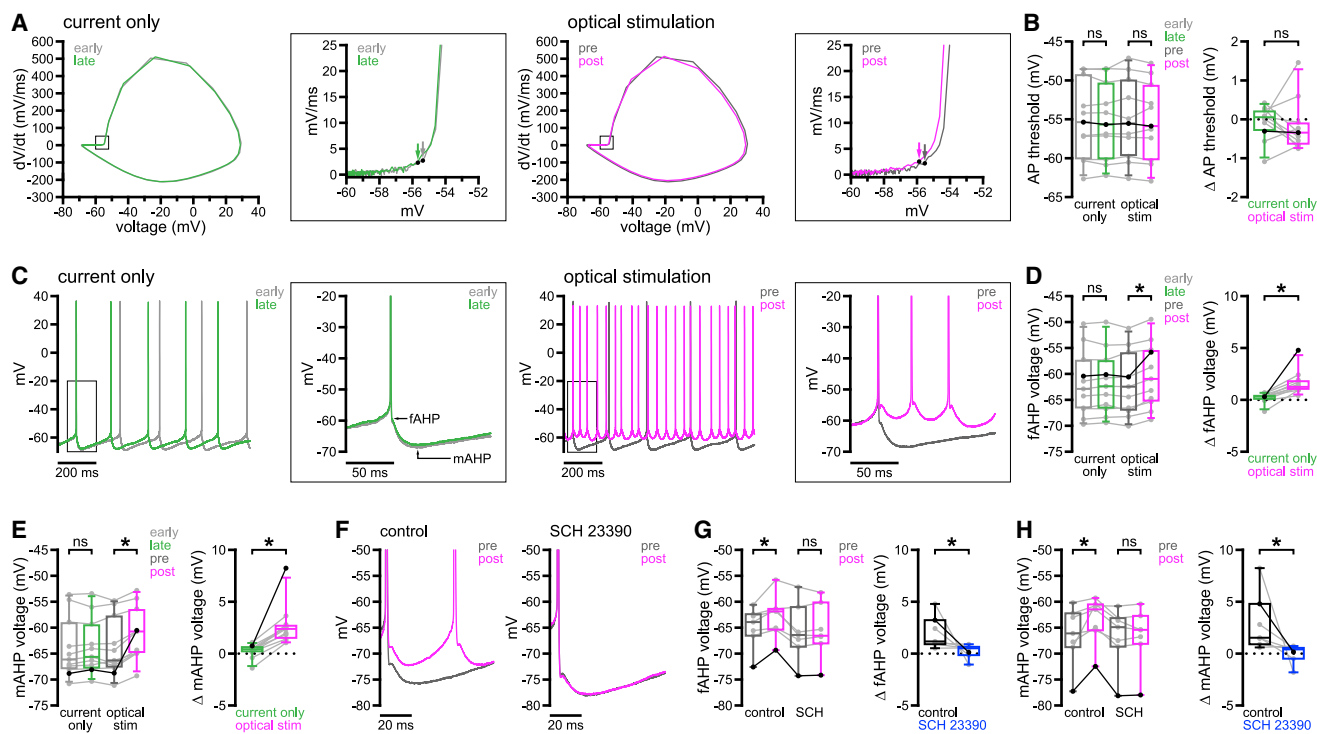


Figure 6. Dopaminergic Modulation Acutely Reduces fAHP and mAHP Amplitudes without Changing Action Potential Threshold

(A and B) Dopaminergic transmission had no effect on action potential threshold during the long up-state protocol (A, example phase plots [arrows denote threshold]; B, population data with bold lines indicating example in A]).

(C–E) Dopaminergic modulation acutely reduced fAHPs and mAHPs (C, example; D and E, population data with bold lines indicating example in C)).

(F–H) Acute modulation of fAHPs and mAHPs was prevented by application of 0.5 μ M SCH 23390 (F, example; G and H, population data with bold lines indicating example in F)).

* $p < 0.05$; ns, not significant.

See also Figure S5 and Tables S7 and S8.

8H). In contrast, threshold hyperpolarized in the presence of Ap/IbTX (Figures 8I and 8J). Although α -DTX did not consistently alter AHP amplitudes (Figures 8K, 8M, and 8N), changes in threshold were strongly correlated with changes in both fAHPs and mAHPs (Figure 8O). Combined effects on threshold and AHPs may therefore explain the increased excitability following application of α -DTX, similar to the persistent effects of dopaminergic modulation. As expected, both fAHPs and mAHPs were reduced in the presence of Ap/IbTX (Figures 8L, 8P, and 8Q), but only mAHP shifts were correlated with changes in threshold (Figure 8R). Because AHP amplitudes were also reduced acutely following dopaminergic transmission, but not persistently in response to DA or consistently following application of α -DTX, these results suggest that negative modulation of Ca_{v2} channels may contribute to the earliest phase of dopaminergic modulation. Together, these data confirm that the major effects of dopaminergic transmission on D1-SPN firing properties are reproduced by inhibition of K_v1 - or Ca_{v2} -associated currents.

DISCUSSION

This study is the first to demonstrate that physiological patterns of nigrostriatal dopaminergic transmission consistently, rapidly, persistently, and powerfully augment up-state firing of

D1-SPNs in the adult DLS. Furthermore, these effects are D1R dependent, occur whether neurons are in the up or down state at the time of transmission, and are consistent with the modulation of postsynaptic voltage- and Ca^{2+} -dependent K^+ conductances rather than $\text{Kir}2$, Ca_v1 , or Na_v1 channels.

Nature and Dynamics of D1-SPN Dopaminergic Modulation

In response to application of exogenous DA or D1R agonists, previous studies have reported mixed effects on D1-SPN firing evoked from up- or down-state membrane potentials. This lack of consensus likely resulted from several factors, including (1) different modes and concentrations of DA or D1R agonist application, typically over sustained periods; (2) invasive intracellular or whole-cell recording techniques that disrupt GPCR signaling and intrinsic properties; and (3) varying methods used to identify D1-SPNs. In contrast, our investigation of native dopaminergic transmission using minimally invasive perforated-patch recordings of genetically identified D1-SPNs revealed consistent positive modulation of up-state firing regardless of initial membrane state. These approaches also enabled us to assess the dynamics and targets of native modulation, which cannot be directly addressed through exogenous agonist application or viral expression of alien effectors (Marcott et al., 2014). As

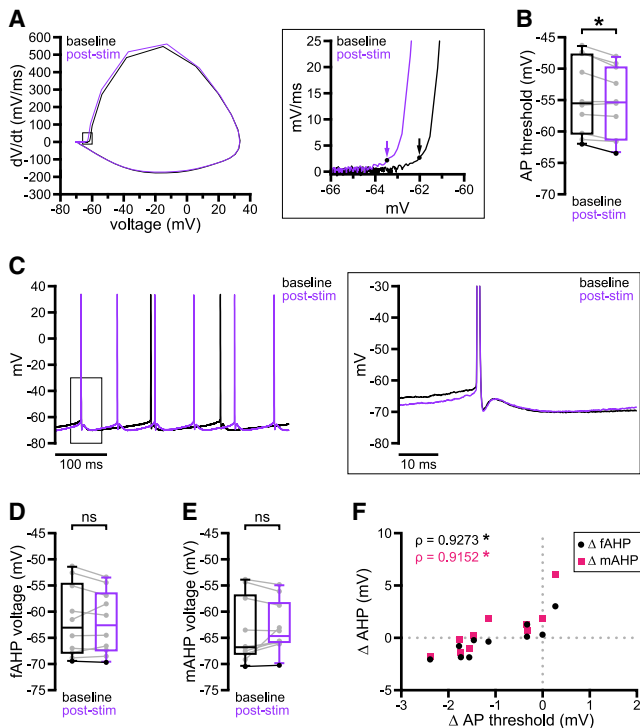


Figure 7. Persistent Dopaminergic Modulation Is Associated with a Reduction in Action Potential Threshold

(A–F) 1 min after optogenetic stimulation, D1-SPN action potential threshold was consistently hyperpolarized relative to baseline (A; example phase plots [arrows denote threshold]; B; population data with bold line indicating example in A]). In contrast, fAHPs and mAHPs were not consistently modulated across the sample population (C; example cell shown in A; D and E; population data with bold lines indicating example in C)). However, changes in fAHPs and mAHPs were correlated with changes in action potential threshold (F; population data).

* $p < 0.05$; ns, not significant; p , Spearman rank correlation coefficient.

See also Table S9.

such, we found that D1-SPN firing rates substantially and persistently increased within hundreds of milliseconds of optogenetically evoked DA release. This is consistent with recent studies suggesting that SN DA neuron activity promotes the initiation and invigoration of action sequences on the sub- to multi-second timescale (da Silva et al., 2018; Howe and Dombeck, 2016). Whether the synchronous release of DA generated by optogenetic stimulation in these and our experiments is equivalent to that occurring normally remains to be determined (Coddington and Dudman, 2018). However, the levels of DA we observed are similar to those measured in the dorsal striatum during natural behavior (Robinson et al., 2002), and brief optogenetic inhibition of SN DA neurons unequivocally impairs the initiation and vigor of subsequent actions (da Silva et al., 2018).

Interestingly, we found that the intrinsic excitability of D1-SPNs remained elevated for minutes following a single bout of optogenetic stimulation. This agrees with a report demonstrating sustained elevation of D1R-mediated PKA activity in SPN somata following transient stimulation of DA axons (Ma et al., 2018), arguing that nigrostriatal dopaminergic signaling

may persistently invigorate selected actions despite rapid, DAT-mediated clearance of extracellular DA (O'Neill et al., 2017; Sulzer et al., 2016). The phasic activity of SN DA neurons is also thought to instruct striatal synaptic plasticity within a more narrow time frame. Consistent with this function, dopaminergic transmission generates relatively brief PKA transients in D1-SPN distal dendrites and spines due to high local phosphodiesterase activity, which restricts the time window for glutamatergic synaptic plasticity (Yagishita et al., 2014). While the potentiation of glutamatergic synapses may require NMDA receptors and D1Rs to be activated in close succession (Yagishita et al., 2014), our data suggest that phasic dopaminergic transmission could also, through its persistent elevation of D1-SPN excitability, facilitate spike timing-dependent plasticity (Berke, 2018; Gerfen and Surmeier, 2011).

Putative Ion Channel Targets of SPN D1R Modulation

Although exogenous agonist activation of SPN D1Rs has been reported to modulate multiple ion channels, only a subset of these appear to be targeted by native dopaminergic transmission. The acceleration of D1-SPN down- to up-state transitions and increased firing frequency are consistent with negative modulation of $K_v1.2$ -containing channels underlying I_{AS} . Indeed, each of these effects is reproduced by pharmacological inhibition of $K_v1.2$ -containing channels (Figure 8; Nisenbaum et al., 1994; Shen et al., 2004). While D1R-mediated negative modulation of $Ca_v2.1$ and $Ca_v2.2$ channels (Surmeier et al., 1995) could not account for the reduced latency to fire, it could contribute to AHP reduction, interspike interval depolarization, and elevation of firing. This subset of effects is reproduced by inhibition of BK and/or SK channels underlying fAHP and mAHP currents, or by blockade of their functionally coupled Ca_v2 channels (Figure 8; Pérez-García et al., 2003; Pineda et al., 1992; Vilchis et al., 2000). Interestingly, acute and persistent dopaminergic modulation were associated primarily with reductions in AHP amplitudes or action potential threshold, respectively. This observation suggests that the relative contribution of ion channels mediating native dopaminergic modulation is more dynamic than previously assumed.

In contrast to the ion channel targets described above, we did not find evidence of functionally significant modulation of Kir2, Na_v1 , or Ca_v1 channels. Although the reported effects of D1R signaling on Kir2 channels have been highly variable (Pacheco-Cano et al., 1996; Podda et al., 2010; Zhao et al., 2016), negative modulation of Na_v1 channels has been consistently reported (Cantrell et al., 1999; Few et al., 2007; Schiffmann et al., 1995; Surmeier et al., 1992). D1R-mediated reduction of peak Na^+ current has been proposed to inhibit down- to up-state transitions. However, we found that the transition to up-state firing was instead enhanced and that action potential threshold was unaffected acutely, and even hyperpolarized persistently, following nigrostriatal stimulation. These findings could reflect the failure of native transmission to significantly modulate Na_v1 channels, the presence of a large reserve of axonal Na_v1 channels, and/or compensatory effects on threshold by modulation of other ion channels (e.g., Ca_v2 and/or $K_v1.2$ -containing channels). D1R signaling has also been linked to the enhancement of Ca_v1 channel currents, and this mechanism was proposed to underlie

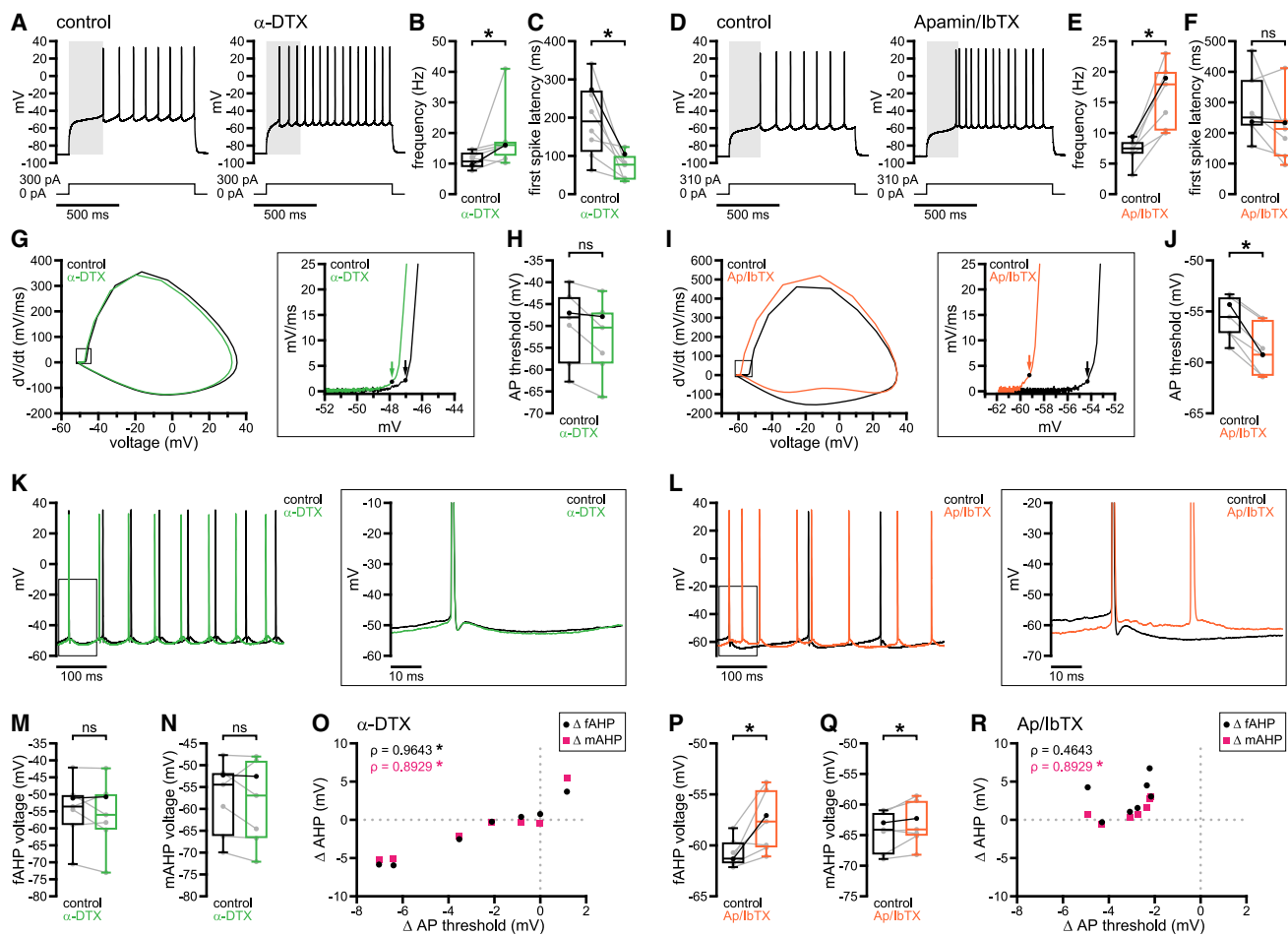


Figure 8. Aspects of Dopaminergic Modulation Are Mimicked by Inhibition of Either Kv1 or SK and BK Channels

(A–F) Application of either α -DTX (A–C) or Ap/IbTX (D–F) enhanced D1-SPN firing frequency, but only α -DTX reduced the latency to fire (A and D, examples; B and C, population data with bold lines indicating example in A; E and F, population data with bold lines indicating example in D; A and D, gray highlight denotes the latency to fire under control conditions).

(G–J) Action potential threshold was not consistently altered by application of α -DTX (G and H) but was markedly reduced in the presence of Ap/IbTX (I and J) (G and I, example phase plots [arrows denote threshold]; H and J, population data with bold lines indicating examples in G and I, respectively).

(K–R) Although fAHP and mAHP amplitudes were not consistently altered in the presence of α -DTX, changes in either were correlated with changes in action potential threshold (K and M–O). In contrast, both fAHPs and mAHPs were reduced in the presence of Ap/IbTX, but only mAHP shifts were correlated with threshold changes (L and P–R) (K and L, example cells shown in G and I, respectively; M and N, population data with bold lines indicating example in K; P and Q, population data with bold lines indicating example in L; O and R, population data).

* $p < 0.05$; ns, not significant; ρ , Spearman rank correlation coefficient.

See also Table S10.

increased D1-SPN spike discharge in response to sustained depolarization (Hernández-López et al., 1997; Surmeier et al., 1995). Although we observed D1R-mediated increases in spike discharge, these effects were not sensitive to Ca_{v1} channel inhibition by isradipine. Again, this discrepancy could indicate that native dopaminergic transmission is insufficient to modulate Ca_{v1} channels or that previous recording conditions or approaches exaggerated the relative impact of Ca_{v1} channel modulation (Hernández-López et al., 1997; Surmeier et al., 1995). Our findings do not exclude the possibility that Ca_{v1} currents are enhanced or that their modulation may be involved in processes we did not measure, like dendritic integration (Flores-Barrera et al., 2011; Vergara et al., 2003).

$\text{K}_{v4.2}$ channels underlie a fast A-type K^+ current that influences subthreshold excitability and firing in SPNs (Carrillo-Reid et al., 2019; Tkatch et al., 2000). Although dopaminergic regulation of these channels has not been reported in SPNs (Day et al., 2008; Surmeier and Kitai, 1993), PKA downregulates $\text{K}_{v4.2}$ -mediated currents in other cell types (Hoffman and Johnston, 1998). Furthermore, genetic deletion of $\text{K}_{v4.2}$ channels enhances SPN excitability (Carrillo-Reid et al., 2019) in a manner similar to that reported here. If D1R signaling negatively modulates $\text{K}_{v4.2}$ channels in SPNs, and if the underlying mechanisms are sensitive to whole-cell dialysis, this effect may have been missed in earlier studies. Therefore, we cannot exclude the possibility that $\text{K}_{v4.2}$ channel modulation contributed to the

elevation of excitability that we observed using perforated-patch recordings.

Application of α -DTX or Ap/IbTX mimicked various aspects of acute and persistent dopaminergic modulation. However, definitive identification of the ion channels underlying D1-SPN excitability changes following synaptic release of DA is challenging. Drugs used to characterize the targets of postsynaptic modulation can also affect transmitter release. For example, compounds that selectively block I_{A5} in SPNs (Coetze et al., 1999; Nisenbaum et al., 1994; Surmeier et al., 1991) also substantially amplify DA release (Fulton et al., 2011; Martel et al., 2011). Conversely, pharmacological blockade of $Ca_{v}2$ channels reduces the initial probability of DA release, thus affecting short-term plasticity (Brimblecombe et al., 2015). Although the perforated-patch configuration was necessary to maintain intact D1R-mediated signaling, it is not well suited to the biophysical characterization of modulated ion channels under voltage clamp. Due to the relatively high access resistance and inability to apply intracellular channel-blocking compounds, the perforated configuration allows less effective voltage control than the whole-cell configuration. As a result, this study was performed entirely using the current-clamp technique, which allowed us to interrogate the impact of native dopaminergic transmission on naturalistic D1-SPN firing behavior.

Functional Considerations

SPN up-state transitions *in vivo* are driven by coordinated glutamatergic input onto dendritic shafts and spines, compartments that exhibit active, nonlinear properties (Carter and Sabatini, 2004; Plotkin et al., 2011; Wilson, 1995a, 1995b; Wilson and Kawaguchi, 1996). Although somatic current injection cannot replicate dendritic synaptic input, our data do suggest that similarly sized synaptic potentials arriving at the axosomatic compartment will generate firing with reduced latency and higher frequency following D1R-mediated modulation of $K_{v}1.2$ and $Ca_{v}2$ channels (Gerfen and Surmeier, 2011). Glutamate uncaging or stimulation of corticostriatal afferents, if combined with noninvasive recording techniques, could be used to definitively address the impact of native dopaminergic signaling on D1-SPN dendritic integration and synaptic plasticity.

The rapid enhancement of D1-SPN activity we observed in response to native dopaminergic transmission provides a cellular mechanism that may support movement. However, the concurrent activity of D1- and D2-SPNs is required for the proper initiation and execution of actions (Tecuapetla et al., 2016). Indeed, individual behavioral syllables are encoded by specific combinations of D1- and D2-SPN activity; for example, running is associated with coincident high D1-SPN and low D2-SPN activity (Markowitz et al., 2018). It remains to be determined whether nigrostriatal inputs negatively modulate D2-SPNs with a time course similar to the positive modulation of D1-SPNs. Given that D1- and D2-SPNs also communicate by lateral inhibition, it will also be critical to understand how native dopaminergic signaling influences their reciprocal synaptic transmission (Burke et al., 2017; Lemos et al., 2016). Our study suggests that noninvasive experimental approaches will be required to address these outstanding questions.

STAR★METHODS

Detailed methods are provided in the online version of this paper and include the following:

- KEY RESOURCES TABLE
- LEAD CONTACT AND MATERIALS AVAILABILITY
- EXPERIMENTAL MODEL AND SUBJECT DETAILS
 - Animals
- METHOD DETAILS
 - Stereotaxic injection of AAV
 - Slice preparation
 - Electrophysiology and optogenetic stimulation
 - Fast-scan cyclic voltammetry (FSCV)
 - Immunohistochemistry and confocal imaging
- QUANTIFICATION AND STATISTICAL ANALYSIS
- DATA AND CODE AVAILABILITY

SUPPLEMENTAL INFORMATION

Supplemental Information can be found online at <https://doi.org/10.1016/j.neuron.2020.01.028>.

ACKNOWLEDGMENTS

This study was funded by NIH NINDS grants P50 NS047085, R37 NS041280, and F31 NS100357. Confocal imaging work was performed at the Northwestern University Center for Advanced Microscopy, which is supported by NIH NCI grant CCSG P30 CA060553 (awarded to the Robert H. Lurie Comprehensive Cancer Center). The authors thank C.J. Wilson, J.D. Berke, D.J. Surmeier, Y. Kozorovitskiy, R.J. Miller, and the rest of the Bevan lab for comments on this study. The authors also thank K.M. Wassum and A.L. Collins for training in FSCV, as well as D.J. Surmeier, D.R. Schowalter, and B.M. Erjavec for providing transgenic DAT^{lRES-Cre} and *Drd1a-tdTomato* breeding mice.

AUTHOR CONTRIBUTIONS

Conceptualization, A.K.L. and M.D.B.; Methodology, A.K.L. and M.D.B.; Formal Analysis, A.K.L.; Investigation, A.K.L. and M.D.B.; Writing – Original Draft, A.K.L. and M.D.B.; Writing – Review & Editing, A.K.L. and M.D.B.; Visualization, A.K.L. and M.D.B.; Supervision, Project Administration, and Funding Acquisition, A.K.L. and M.D.B.

DECLARATION OF INTERESTS

The authors declare no competing interests.

Received: April 18, 2019

Revised: December 26, 2019

Accepted: January 22, 2020

Published: February 18, 2020

REFERENCES

- Ade, K.K., Wan, Y., Chen, M., Gloss, B., and Calakos, N. (2011). An improved BAC transgenic fluorescent reporter line for sensitive and specific identification of striatonigral medium spiny neurons. *Front. Syst. Neurosci.* 5, 32.
- Bäckman, C.M., Malik, N., Zhang, Y., Shan, L., Grinberg, A., Hoffer, B.J., Westphal, H., and Tomac, A.C. (2006). Characterization of a mouse strain expressing Cre recombinase from the 3' untranslated region of the dopamine transporter locus. *Genesis* 44, 383–390.
- Barry, P.H. (1994). JPCalc, a software package for calculating liquid junction potential corrections in patch-clamp, intracellular, epithelial and bilayer

- measurements and for correcting junction potential measurements. *J. Neurosci. Methods* 51, 107–116.
- Barter, J.W., Li, S., Lu, D., Bartholomew, R.A., Rossi, M.A., Shoemaker, C.T., Salas-Meza, D., Gaidis, E., and Yin, H.H. (2015). Beyond reward prediction errors: the role of dopamine in movement kinematics. *Front. Integr. Nuerosci.* 9, 39.
- Bass, C.E., Grinevich, V.P., Kulikova, A.D., Bonin, K.D., and Budygin, E.A. (2013). Terminal effects of optogenetic stimulation on dopamine dynamics in rat striatum. *J. Neurosci. Methods* 214, 149–155.
- Baufreton, J., Atherton, J.F., Surmeier, D.J., and Bevan, M.D. (2005). Enhancement of excitatory synaptic integration by GABAergic inhibition in the subthalamic nucleus. *J. Neurosci.* 25, 8505–8517.
- Beaulieu, J.M., and Gainetdinov, R.R. (2011). The physiology, signaling, and pharmacology of dopamine receptors. *Pharmacol. Rev.* 63, 182–217.
- Berke, J.D. (2018). What does dopamine mean? *Nat. Neurosci.* 21, 787–793.
- Bracci, E., and Panzeri, S. (2006). Excitatory GABAergic effects in striatal projection neurons. *J. Neurophysiol.* 95, 1285–1290.
- Brimblecombe, K.R., Gracie, C.J., Platt, N.J., and Cragg, S.J. (2015). Gating of dopamine transmission by calcium and axonal N-, Q-, T- and L-type voltage-gated calcium channels differs between striatal domains. *J. Physiol.* 593, 929–946.
- Bucher, E.S., Brooks, K., Verber, M.D., Keithley, R.B., Owesson-White, C., Carroll, S., Takmakov, P., McKinney, C.J., and Wightman, R.M. (2013). Flexible software platform for fast-scan cyclic voltammetry data acquisition and analysis. *Anal. Chem.* 85, 10344–10353.
- Burke, D.A., Rotstein, H.G., and Alvarez, V.A. (2017). Striatal local circuitry: a new framework for lateral inhibition. *Neuron* 96, 267–284.
- Calabresi, P., Mercuri, N., Stanzione, P., Stefani, A., and Bernardi, G. (1987). Intracellular studies on the dopamine-induced firing inhibition of neostriatal neurons *in vitro*: evidence for D1 receptor involvement. *Neuroscience* 20, 757–771.
- Cantrell, A.R., Scheuer, T., and Catterall, W.A. (1999). Voltage-dependent neuromodulation of Na^+ channels by D1-like dopamine receptors in rat hippocampal neurons. *J. Neurosci.* 19, 5301–5310.
- Carrillo-Reid, L., Day, M., Xie, Z., Melendez, A.E., Kondapalli, J., Plotkin, J.L., Wokosin, D.L., Chen, Y., Kress, G.J., Kaplitt, M., et al. (2019). Mutant huntingtin enhances activation of dendritic Kv4 K^+ channels in striatal spiny projection neurons. *eLife* 8, e40818.
- Carter, A.G., and Sabatini, B.L. (2004). State-dependent calcium signaling in dendritic spines of striatal medium spiny neurons. *Neuron* 44, 483–493.
- Chuhma, N., Mingote, S., Kalmbach, A., Yetnikoff, L., and Rapoport, S. (2017). Heterogeneity in dopamine neuron synaptic actions across the striatum and its relevance for schizophrenia. *Biol. Psychiatry* 81, 43–51.
- Clark, J.J., Sandberg, S.G., Wanat, M.J., Gan, J.O., Horne, E.A., Hart, A.S., Akers, C.A., Parker, J.G., Willuhn, I., Martinez, V., et al. (2010). Chronic micro-sensors for longitudinal, subsecond dopamine detection in behaving animals. *Nat. Methods* 7, 126–129.
- Coddington, L.T., and Dudman, J.T. (2018). The timing of action determines reward prediction signals in identified midbrain dopamine neurons. *Nat. Neurosci.* 21, 1563–1573.
- Coetzee, W.A., Amarillo, Y., Chiu, J., Chow, A., Lau, D., McCormack, T., Moreno, H., Nadal, M.S., Ozaita, A., Pountney, D., et al. (1999). Molecular diversity of K^+ channels. *Ann. N Y Acad. Sci.* 868, 233–285.
- Cui, G., Jun, S.B., Jin, X., Pham, M.D., Vogel, S.S., Lovinger, D.M., and Costa, R.M. (2013). Concurrent activation of striatal direct and indirect pathways during action initiation. *Nature* 494, 238–242.
- da Silva, J.A., Tecuapetla, F., Paixão, V., and Costa, R.M. (2018). Dopamine neuron activity before action initiation gates and invigorates future movements. *Nature* 554, 244–248.
- Day, M., Wokosin, D., Plotkin, J.L., Tian, X., and Surmeier, D.J. (2008). Differential excitability and modulation of striatal medium spiny neuron dendrites. *J. Neurosci.* 28, 11603–11614.
- Few, W.P., Scheuer, T., and Catterall, W.A. (2007). Dopamine modulation of neuronal Na^+ channels requires binding of A kinase-anchoring protein 15 and PKA by a modified leucine zipper motif. *Proc. Natl. Acad. Sci. USA* 104, 5187–5192.
- Fiorillo, C.D., and Williams, J.T. (1998). Glutamate mediates an inhibitory postsynaptic potential in dopamine neurons. *Nature* 394, 78–82.
- Flores-Barrera, E., Vizcarra-Chacón, B.J., Bargas, J., Tapia, D., and Galarraga, E. (2011). Dopaminergic modulation of corticostriatal responses in medium spiny projection neurons from direct and indirect pathways. *Front. Syst. Neurosci.* 5, 15.
- Freeze, B.S., Kravitz, A.V., Hammack, N., Berke, J.D., and Kreitzer, A.C. (2013). Control of basal ganglia output by direct and indirect pathway projection neurons. *J. Neurosci.* 33, 18531–18539.
- Fulton, S., Thibault, D., Mendez, J.A., Lahiae, N., Tirotta, E., Borrelli, E., Bouvier, M., Tempel, B.L., and Trudeau, L.E. (2011). Contribution of Kv1.2 voltage-gated potassium channel to D2 autoreceptor regulation of axonal dopamine overflow. *J. Biol. Chem.* 286, 9360–9372.
- Gabel, L.A., and Nisenbaum, E.S. (1998). Biophysical characterization and functional consequences of a slowly inactivating potassium current in neostriatal neurons. *J. Neurophysiol.* 79, 1989–2002.
- Gainetdinov, R.R., Premont, R.T., Bohn, L.M., Lefkowitz, R.J., and Caron, M.G. (2004). Desensitization of G protein-coupled receptors and neuronal functions. *Annu. Rev. Neurosci.* 27, 107–144.
- Gerfen, C.R., and Surmeier, D.J. (2011). Modulation of striatal projection systems by dopamine. *Annu. Rev. Neurosci.* 34, 441–466.
- Gervasi, N., Hepp, R., Tricoire, L., Zhang, J., Lambolez, B., Paupardin-Tritsch, D., and Vincent, P. (2007). Dynamics of protein kinase A signaling at the membrane, in the cytosol, and in the nucleus of neurons in mouse brain slices. *J. Neurosci.* 27, 2744–2750.
- Grace, A.A., and Bunney, B.S. (1984a). The control of firing pattern in nigral dopamine neurons: single spike firing. *J. Neurosci.* 4, 2866–2876.
- Grace, A.A., and Bunney, B.S. (1984b). The control of firing pattern in nigral dopamine neurons: burst firing. *J. Neurosci.* 4, 2877–2890.
- Greengard, P. (2001). The neurobiology of slow synaptic transmission. *Science* 294, 1024–1030.
- Hernández-López, S., Bargas, J., Surmeier, D.J., Reyes, A., and Galarraga, E. (1997). D1 receptor activation enhances evoked discharge in neostriatal medium spiny neurons by modulating an L-type Ca^{2+} conductance. *J. Neurosci.* 17, 3334–3342.
- Hoffman, D.A., and Johnston, D. (1998). Downregulation of transient K^+ channels in dendrites of hippocampal CA1 pyramidal neurons by activation of PKA and PKC. *J. Neurosci.* 18, 3521–3528.
- Holm, S. (1979). A simple sequentially rejective multiple test procedure. *Scand. J. Stat.* 6, 65–70.
- Horn, R., and Marty, A. (1988). Muscarinic activation of ionic currents measured by a new whole-cell recording method. *J. Gen. Physiol.* 92, 145–159.
- Howe, M.W., and Dombeck, D.A. (2016). Rapid signalling in distinct dopaminergic axons during locomotion and reward. *Nature* 535, 505–510.
- Kim, J.I., Ganesan, S., Luo, S.X., Wu, Y.W., Park, E., Huang, E.J., Chen, L., and Ding, J.B. (2015). Aldehyde dehydrogenase 1a1 mediates a GABA synthesis pathway in midbrain dopaminergic neurons. *Science* 350, 102–106.
- Kravitz, A.V., Freeze, B.S., Parker, P.R., Kay, K., Thwin, M.T., Deisseroth, K., and Kreitzer, A.C. (2010). Regulation of parkinsonian motor behaviours by optogenetic control of basal ganglia circuitry. *Nature* 466, 622–626.
- Kyrozis, A., and Reichling, D.B. (1995). Perforated-patch recording with gramicidin avoids artifactual changes in intracellular chloride concentration. *J. Neurosci. Methods* 57, 27–35.
- Lemos, J.C., Friend, D.M., Kaplan, A.R., Shin, J.H., Rubenstein, M., Kravitz, A.V., and Alvarez, V.A. (2016). Enhanced GABA transmission drives bradykinesia following loss of dopamine D2 receptor signaling. *Neuron* 90, 824–838.

- Lindroos, R., Dorst, M.C., Du, K., Filipović, M., Keller, D., Ketze, M., Kozlov, A.K., Kumar, A., Lindahl, M., Nair, A.G., et al. (2018). Basal ganglia neuromodulation over multiple temporal and structural scales—simulations of direct pathway MSNs investigate the fast onset of dopaminergic effects and predict the role of Kv4.2. *Front. Neural Circuits* 12, 3.
- Lu, Y., Driscoll, N., Ozden, I., Yu, Z., and Nurmikko, A.V. (2015). Modulating dopamine release by optogenetics in transgenic mice reveals terminal dopaminergic dynamics. *Neurophotonics* 2, 031207.
- Ma, L., Jongbloets, B.C., Xiong, W.H., Melander, J.B., Qin, M., Lameyer, T.J., Harrison, M.F., Zemelman, B.V., Mao, T., and Zhong, H. (2018). A highly sensitive A-kinase activity reporter for imaging neuromodulatory events in awake mice. *Neuron* 99, 665–679.e5.
- Marcott, P.F., Mamaligas, A.A., and Ford, C.P. (2014). Phasic dopamine release drives rapid activation of striatal D2-receptors. *Neuron* 84, 164–176.
- Marinelli, M., and McCutcheon, J.E. (2014). Heterogeneity of dopamine neuron activity across traits and states. *Neuroscience* 282, 176–197.
- Markowitz, J.E., Gillis, W.F., Beron, C.C., Neufeld, S.Q., Robertson, K., Bhagat, N.D., Peterson, R.E., Peterson, E., Hyun, M., Linderman, S.W., et al. (2018). The striatum organizes 3D behavior via moment-to-moment action selection. *Cell* 174, 44–58.e17.
- Martel, P., Leo, D., Fulton, S., Bérard, M., and Trudeau, L.E. (2011). Role of Kv1 potassium channels in regulating dopamine release and presynaptic D2 receptor function. *PLoS ONE* 6, e20402.
- Mazzoni, P., Hristova, A., and Krakauer, J.W. (2007). Why don't we move faster? Parkinson's disease, movement vigor, and implicit motivation. *J. Neurosci.* 27, 7105–7116.
- Melchior, J.R., Ferris, M.J., Stuber, G.D., Riddle, D.R., and Jones, S.R. (2015). Optogenetic versus electrical stimulation of dopamine terminals in the nucleus accumbens reveals local modulation of presynaptic release. *J. Neurochem.* 134, 833–844.
- Mink, J.W. (1996). The basal ganglia: focused selection and inhibition of competing motor programs. *Prog. Neurobiol.* 50, 381–425.
- Neher, E. (1992). Correction for liquid junction potentials in patch clamp experiments. *Methods Enzymol.* 207, 123–131.
- Nicola, S.M., Surmeier, J., and Malenka, R.C. (2000). Dopaminergic modulation of neuronal excitability in the striatum and nucleus accumbens. *Annu. Rev. Neurosci.* 23, 185–215.
- Nisenbaum, E.S., and Wilson, C.J. (1995). Potassium currents responsible for inward and outward rectification in rat neostriatal spiny projection neurons. *J. Neurosci.* 15, 4449–4463.
- Nisenbaum, E.S., Xu, Z.C., and Wilson, C.J. (1994). Contribution of a slowly inactivating potassium current to the transition to firing of neostriatal spiny projection neurons. *J. Neurophysiol.* 71, 1174–1189.
- Nisenbaum, E.S., Wilson, C.J., Foehring, R.C., and Surmeier, D.J. (1996). Isolation and characterization of a persistent potassium current in neostriatal neurons. *J. Neurophysiol.* 76, 1180–1194.
- O'Neill, B., Patel, J.C., and Rice, M.E. (2017). Characterization of optically and electrically evoked dopamine release in striatal slices from digenic knock-in mice with DAT-driven expression of channelrhodopsin. *ACS Chem. Neurosci.* 8, 310–319.
- Pacheco-Cano, M.T., Bargas, J., Hernández-López, S., Tapia, D., and Galarraga, E. (1996). Inhibitory action of dopamine involves a subthreshold Cs⁺-sensitive conductance in neostriatal neurons. *Exp. Brain Res.* 110, 205–211.
- Panigrahi, B., Martin, K.A., Li, Y., Graves, A.R., Vollmer, A., Olson, L., Mensh, B.D., Karpova, A.Y., and Dudman, J.T. (2015). Dopamine is required for the neural representation and control of movement vigor. *Cell* 162, 1418–1430.
- Patriarchi, T., Cho, J.R., Merten, K., Howe, M.W., Marley, A., Xiong, W.H., Folk, R.W., Broussard, G.J., Liang, R., Jang, M.J., et al. (2018). Ultrafast neuronal imaging of dopamine dynamics with designed genetically encoded sensors. *Science* 360, eaat4422.
- Pérez-Garci, E., Bargas, J., and Galarraga, E. (2003). The role of Ca²⁺ channels in the repetitive firing of striatal projection neurons. *Neuroreport* 14, 1253–1256.
- Pineda, J.C., Galarraga, E., Bargas, J., Cristancho, M., and Aceves, J. (1992). Charybdotoxin and apamin sensitivity of the calcium-dependent repolarization and the afterhyperpolarization in neostriatal neurons. *J. Neurophysiol.* 68, 287–294.
- Plotkin, J.L., Day, M., and Surmeier, D.J. (2011). Synaptically driven state transitions in distal dendrites of striatal spiny neurons. *Nat. Neurosci.* 14, 881–888.
- Podda, M.V., Riccardi, E., D'Ascenzo, M., Azzena, G.B., and Grassi, C. (2010). Dopamine D1-like receptor activation depolarizes medium spiny neurons of the mouse nucleus accumbens by inhibiting inwardly rectifying K⁺ currents through a cAMP-dependent protein kinase A-independent mechanism. *Neuroscience* 167, 678–690.
- Ramos, M., Goñi-Allo, B., and Aguirre, N. (2005). Administration of SCH 23390 into the medial prefrontal cortex blocks the expression of MDMA-induced behavioral sensitization in rats: an effect mediated by 5-HT_{2C} receptor stimulation and not by D1 receptor blockade. *Neuropsychopharmacology* 30, 2180–2191.
- Robinson, D.L., Heien, M.L., and Wightman, R.M. (2002). Frequency of dopamine concentration transients increases in dorsal and ventral striatum of male rats during introduction of conspecifics. *J. Neurosci.* 22, 10477–10486.
- Roseberry, T.K., Lee, A.M., Lalive, A.L., Wilbrecht, L., Bonci, A., and Kreitzer, A.C. (2016). Cell-type-specific control of brainstem locomotor circuits by basal ganglia. *Cell* 164, 526–537.
- Schiffmann, S.N., Lledo, P.M., and Vincent, J.D. (1995). Dopamine D1 receptor modulates the voltage-gated sodium current in rat striatal neurones through a protein kinase A. *J. Physiol.* 483, 95–107.
- Schindelin, J., Arganda-Carreras, I., Frise, E., Kaynig, V., Longair, M., Pietzsch, T., Preibisch, S., Rueden, C., Saalfeld, S., Schmid, B., et al. (2012). Fiji: an open-source platform for biological-image analysis. *Nat. Methods* 9, 676–682.
- Shen, W., Hernández-López, S., Tkatch, T., Held, J.E., and Surmeier, D.J. (2004). Kv1.2-containing K⁺ channels regulate subthreshold excitability of striatal medium spiny neurons. *J. Neurophysiol.* 91, 1337–1349.
- Shen, W., Tian, X., Day, M., Ulrich, S., Tkatch, T., Nathanson, N.M., and Surmeier, D.J. (2007). Cholinergic modulation of Kir2 channels selectively elevates dendritic excitability in striatopallidal neurons. *Nat. Neurosci.* 10, 1458–1466.
- Sulzer, D., Cragg, S.J., and Rice, M.E. (2016). Striatal dopamine neurotransmission: regulation of release and uptake. *Basal Ganglia* 6, 123–148.
- Surmeier, D.J., and Kitai, S.T. (1993). D1 and D2 dopamine receptor modulation of sodium and potassium currents in rat neostriatal neurons. *Prog. Brain Res.* 99, 309–324.
- Surmeier, D.J., Stefani, A., Foehring, R.C., and Kitai, S.T. (1991). Developmental regulation of a slowly-inactivating potassium conductance in rat neostriatal neurons. *Neurosci. Lett.* 122, 41–46.
- Surmeier, D.J., Eberwine, J., Wilson, C.J., Cao, Y., Stefani, A., and Kitai, S.T. (1992). Dopamine receptor subtypes colocalize in rat striatonigral neurons. *Proc. Natl. Acad. Sci. USA* 89, 10178–10182.
- Surmeier, D.J., Bargas, J., Hemmings, H.C., Jr., Nairn, A.C., and Greengard, P. (1995). Modulation of calcium currents by a D1 dopaminergic protein kinase/phosphatase cascade in rat neostriatal neurons. *Neuron* 14, 385–397.
- Surmeier, D.J., Ding, J., Day, M., Wang, Z., and Shen, W. (2007). D1 and D2 dopamine-receptor modulation of striatal glutamatergic signaling in striatal medium spiny neurons. *Trends Neurosci.* 30, 228–235.
- Tecuapetla, F., Jin, X., Lima, S.Q., and Costa, R.M. (2016). Complementary contributions of striatal projection pathways to action initiation and execution. *Cell* 166, 703–715.
- Tkatch, T., Baranauskas, G., and Surmeier, D.J. (2000). Kv4.2 mRNA abundance and A-type K⁺ current amplitude are linearly related in basal ganglia and basal forebrain neurons. *J. Neurosci.* 20, 579–588.

- Tritsch, N.X., Ding, J.B., and Sabatini, B.L. (2012). Dopaminergic neurons inhibit striatal output through non-canonical release of GABA. *Nature* **490**, 262–266.
- Trudeau, L.E., Hnasko, T.S., Wallén-Mackenzie, A., Morales, M., Rayport, S., and Sulzer, D. (2014). The multilingual nature of dopamine neurons. *Prog. Brain Res.* **211**, 141–164.
- Vergara, R., Rick, C., Hernández-López, S., Laville, J.A., Guzman, J.N., Galarraga, E., Surmeier, D.J., and Bargas, J. (2003). Spontaneous voltage oscillations in striatal projection neurons in a rat corticostriatal slice. *J. Physiol.* **553**, 169–182.
- Vilchis, C., Bargas, J., Ayala, G.X., Galván, E., and Galarraga, E. (2000). Ca^{2+} channels that activate Ca^{2+} -dependent K^+ currents in neostriatal neurons. *Neuroscience* **95**, 745–752.
- Wilcox, R.R., and Rousselet, G.A. (2018). A guide to robust statistical methods in neuroscience. *Curr. Protoc. Neurosci.* **82**, 8.42.1–8.42.30.
- Wilson, C.J. (1993). The generation of natural firing patterns in neostriatal neurons. *Prog. Brain Res.* **99**, 277–297.
- Wilson, C.J. (1995a). Dynamic modification of dendritic cable properties and synaptic transmission by voltage-gated potassium channels. *J. Comput. Neurosci.* **2**, 91–115.
- Wilson, C.J. (1995b). The contribution of cortical neurons to the firing pattern of striatal spiny neurons. In *Models of Information Processing in the Basal Ganglia*, J.C. Houk, J.L. Davis, and D.G. Beiser, eds. (MIT Press), pp. 29–50.
- Wilson, C.J., and Kawaguchi, Y. (1996). The origins of two-state spontaneous membrane potential fluctuations of neostriatal spiny neurons. *J. Neurosci.* **16**, 2397–2410.
- Yagishita, S., Hayashi-Takagi, A., Ellis-Davies, G.C., Urakubo, H., Ishii, S., and Kasai, H. (2014). A critical time window for dopamine actions on the structural plasticity of dendritic spines. *Science* **345**, 1616–1620.
- Zhao, B., Zhu, J., Dai, D., Xing, J., He, J., Fu, Z., Zhang, L., Li, Z., and Wang, W. (2016). Differential dopaminergic regulation of inwardly rectifying potassium channel mediated subthreshold dynamics in striatal medium spiny neurons. *Neuropharmacology* **107**, 396–410.

STAR★METHODS

KEY RESOURCES TABLE

REAGENT or RESOURCE	SOURCE	IDENTIFIER
Antibodies		
Mouse anti-Tyrosine Hydroxylase monoclonal antibody (clone LNC1)	MilliporeSigma	Cat#MAB318; RRID: AB_2201528
Alexa Fluor 594 donkey anti-mouse IgG (H+L)	Jackson ImmunoResearch Laboratories, Inc.	Cat#715-585-150; RRID: AB_2340854
Alexa Fluor 647 donkey anti-mouse IgG (H+L)	Jackson ImmunoResearch Laboratories, Inc.	Cat#715-605-150; RRID: AB_2340862
Bacterial and Virus Strains		
AAV9.EF1a.DIO.hChR2(H134R)-eYFP.WPRE.hGH	Penn Vector Core	Cat#AV-9-20298P; Addgene 20298-AAV9
Chemicals, Peptides, and Recombinant Proteins		
Alexa Fluor 594 Hydrazide	Thermo Fisher Scientific	Cat#A10438
Apamin	Hello Bio Inc.	Cat#HB1051
Bovine Serum Albumin (BSA)	MilliporeSigma	Cat#A2058
CGP 55845 hydrochloride	Abcam	Cat#ab120337
α-Dendrotoxin (α-DTX)	Alomone Labs	Cat#D-350
D-AP5 (D-APV)	Hello Bio Inc.	Cat#HB0225
DNQX disodium salt	Hello Bio Inc.	Cat#HB0262
Dopamine hydrochloride	Tocris Bioscience	Cat#3548
Gramicidin from <i>Bacillus aneurinolyticus</i>	MilliporeSigma	Cat#G5002
Iberiotoxin	Alomone Labs	Cat#STI-400
Isradipine	Hello Bio Inc.	Cat#HB1223
Mecamylamine hydrochloride	Tocris Bioscience	Cat#2843
PKI 14-22 amide, myristoylated (PKI)	Tocris Bioscience	Cat#2546
RS 102221 hydrochloride	Tocris Bioscience	Cat#1050
SCH 23390 hydrochloride	Tocris Bioscience	Cat#0925
Scopolamine hydrobromide	Tocris Bioscience	Cat#1414
SR 95531 hydrobromide (Gabazine)	Hello Bio Inc.	Cat#HB0901
Deposited Data		
Raw and analyzed data	This paper	Tables S1–S10; https://doi.org/10.17605/OSF.IO/QUW5J
Experimental Models: Organisms/Strains		
Mouse: <i>Drd1a</i> -tdTomato: B6.Cg-Tg(<i>Drd1a</i> -tdTomato)6Calak/J	The Jackson Laboratory	RRID: IMSR_JAX:016204
Mouse: <i>DAT</i> ^{ires-Cre} : B6.SJL-S/c6a3 ^{tm1.1(cre)Bkmn} /J	The Jackson Laboratory	RRID: IMSR_JAX:006660
Software and Algorithms		
Fiji (version 1.52c)	Schindelin et al., 2012	RRID: SCR_002285; https://fiji.sc
HDCV Analysis	Department of Chemistry at the University of North Carolina, Chapel Hill; Bucher et al., 2013	https://chem.unc.edu/critcl-main/critcl-electronics/critcl-electronics-hardware
Origin (version 2016)	OriginLab Corporation	RRID: SCR_014212; https://www.originlab.com
pClamp 10 (versions 10.3, 10.7)	Molecular Devices	RRID: SCR_011323; https://www.moleculardevices.com
Photoshop (version 20.0.2)	Adobe	RRID: SCR_014199; https://www.adobe.com
Prism (version 8.3.0)	GraphPad Software	RRID: SCR_002798; https://www.graphpad.com

LEAD CONTACT AND MATERIALS AVAILABILITY

Further information and requests for resources and reagents should be directed to and will be fulfilled by the Lead Contact, Mark Bevan (m-bevan@northwestern.edu). This study did not generate new unique reagents.

EXPERIMENTAL MODEL AND SUBJECT DETAILS

Animals

Homozygous *DAT*^{lRES-Cre} (RRID: IMSR_JAX:006660) and *Drd1a*-tdTomato (RRID: IMSR_JAX:016204) breeding mice were obtained from the laboratory of D.J. Surmeier at Northwestern University. Homozygotes from each strain were crossed in-house to produce heterozygous, double-transgenic *DAT*^{lRES-Cre/wt},*Drd1a*-tdTomato^{+/−} offspring. Before experimental use, expression of both transgenes was confirmed in at least 6 offspring per breeding pair using real-time PCR (Transnetyx, Inc., Cordova, TN, USA). Adult male (age = 83, 65–105 days; n = 25) and female (age = 79, 64–102 days old; n = 26) *DAT*^{lRES-Cre/+},*Drd1a*-tdTomato^{+/−} mice were used in this study (ages represent median and range). Animals were housed 1–5 per cage, maintained on a 14-hour light/10-hour dark cycle with unrestricted access to food and water, and monitored daily by animal care technicians, veterinarians, and research staff. All procedures were performed with approval of the Institutional Animal Care and Use Committee of Northwestern University, in accordance with national standards established in the Guide for the Care and Use of Laboratory Animals (NRC).

Each experiment was performed on neurons derived from both male and female mice, in approximately equal proportions whenever possible. Although small sample sizes prohibited a formal evaluation of the impact of sex on the results of some experiments, separate analyses of male and female observations for the largest datasets revealed overlapping sample distributions (e.g., for modulation onset time) and no changes in the significance of key results, including the acute and persistent modulation of firing frequency during the long up-state protocol as well as the modulation of spike frequency and latency during the short up-state protocol. In addition, male and female observations did not segregate into bimodal distributions for other datasets. Thus, male and female data were pooled for all experiments presented in this study.

METHOD DETAILS

Stereotaxic injection of AAV

Surgery was performed on *DAT*^{lRES-Cre/wt},*Drd1a*-tdTomato^{+/−} animals at 6–12 weeks of age. Anesthesia was induced by intraperitoneal administration of ketamine (100 mg/kg) and was maintained during surgery by inhalation of 0.5%–2% isoflurane (Smiths Medical ASD, Inc., Dublin, OH, USA). Prior to injection, viral vectors were diluted to an appropriate concentration (determined empirically for each lot) with sterile HEPES-buffered synthetic interstitial fluid (HBS) containing (in mM): 140 NaCl, 23 glucose, 15 HEPES, 3 KCl, 1.5 MgCl₂, 1.6 CaCl₂ (pH 7.2 with NaOH, 300–310 mOsm/kg). Cre-dependent ChR2(H134R)-eYFP expression in nigrostriatal DA neurons was achieved by unilateral or bilateral stereotaxic injection (Neurostar, Tübingen, Germany) of AAV9.EF1a.DIO.hChR2(H134R)-eYFP.WPRE.hGH (diluted to 3.8–7.6 × 10¹¹ genome copies (GC)/mL as described above; Penn Vector Core, Philadelphia, PA, USA) into two sites centered on SN pars compacta (coordinates from Bregma: AP –3.0 mm, ML ± 1.25 mm, DV [from dura] –4.3 mm; AP –2.6 mm, ML ± 1.55, DV [from dura] –4.1 mm). Injections (0.5 μL per site) were delivered via a 10 μL syringe affixed with a 33- or 34-gauge blunt needle (Hamilton Company, Reno, NV, USA) at a rate of 0.1 μL/min, after which the needle was left in place for 10 minutes before removal at a rate of 1–2 mm/min. The scalp was then sutured and animals were maintained on a heating pad until fully recovered from anesthesia. Carprofen (5 mg/kg) was administered subcutaneously for postoperative analgesia over a period of 24–48 hours, including the day of surgery. Brain slices for ex vivo electrophysiology, fast-scan cyclic voltammetry, and/or histology were prepared ~3–4 weeks (23, 20–42 days; n = 51 mice) after surgery.

Slice preparation

Mice expressing ChR2(H134R)-eYFP in SN DA neurons were deeply anesthetized with ketamine/xylazine (> 90/10 mg/kg, IP) and monitored for cessation of reflexes, then transcardially perfused with ice-cold sucrose-based artificial cerebrospinal fluid (sucrose aCSF), equilibrated with 95% O₂ and 5% CO₂ and containing (in mM): 230 sucrose, 26 NaHCO₃, 2.5 KCl, 1.25 NaH₂PO₄, 0.5 CaCl₂, 10 MgSO₄, 10 glucose, 1 Na-pyruvate, and 0.005 L-glutathione. The brain was then blocked in the sagittal plane, removed from the skull, and affixed to the stage of a vibratome (VT1200 S; Leica Biosystems Inc., Buffalo Grove, IL, USA) where it remained submerged in ice-cold, 95% O₂/5% CO₂-equilibrated sucrose aCSF. From each ChR2(H134R)-eYFP-expressing hemisphere, 4–6 parasagittal slices (250 μm thick) containing the lateral half of striatum were collected. Expression of ChR2(H134R)-eYFP was confirmed by brief visual inspection using a dual fluorescent protein flashlight (DFP-1; NIGHTSEA, Lexington, MA, USA). Slices were then transferred to a holding chamber filled with standard aCSF at 35°C, equilibrated with 95% O₂ and 5% CO₂ and containing (in mM): 26 NaHCO₃, 126 NaCl, 2.5 KCl, 1.25 NaH₂PO₄, 2 CaCl₂, 2 MgSO₄, 10 glucose, 1 Na-pyruvate, and 0.005 L-glutathione. Slices were held at 35°C for 30 minutes, after which they were maintained in aCSF at room temperature and protected from light until recording.

Electrophysiology and optogenetic stimulation

Individual slices were transferred to a recording chamber mounted on an upright microscope (Axioskop FS2; Carl Zeiss, Oberkochen, Germany), where they were continuously perfused at a rate of 4–5 mL/min with synthetic interstitial fluid (SIF) warmed to 35°C, equilibrated with 95% O₂ and 5% CO₂ and containing (in mM): 26 NaHCO₃, 126 NaCl, 3 KCl, 1.25 NaH₂PO₄, 1.6 CaCl₂, 1.5 MgSO₄, and 10 glucose. Mecamylamine (5 μM) and scopolamine (1 μM) were routinely added to inhibit nicotinic and muscarinic acetylcholine receptors, respectively. Cholinergic antagonists were present in all recordings with the exception of 7 neurons (out of 115 total); these neurons exhibited no obvious differences in responsiveness to dopaminergic modulation and were thus included in the short up-state dataset (Figures 4, 5I, 6F–6H, and S5G–S5M). In all experiments except those explicitly evaluating amino acidergic co-transmission, SR 95531 (Gabazine, 10 μM), CGP 55845 (2 μM), DNQX (20 μM), and D-APV (50 μM) were also included in the SIF to block GABA_A, GABA_B, AMPA/kainate, and NMDA receptors, respectively. GABAergic and glutamatergic antagonists were added sequentially in co-transmission experiments to confirm the identity of transmitters generating optically evoked IPSPs or EPSPs in the control solution (SIF with cholinergic antagonists only). In experiments employing the D1R antagonist SCH 23390 (0.5 μM), the 5-HT_{2C} antagonist RS 102221 (0.5 μM) was included in both the control and SCH 23390-containing SIF solutions to block the off-target activation of 5-HT_{2C} receptors by SCH 23390 (Ramos et al., 2005). Where indicated, isradipine (5–10 μM) was added to the recording solution to inhibit Ca₁ channel opening. For PKA inhibition experiments, the cell-permeable peptide inhibitor PKI 14-22 amide, myristoylated (PKI, 1 μM) was bath-applied for at least 10 minutes prior to recording; in 3 of 15 recordings, slices were also pre-incubated in aCSF containing 1 μM PKI for ~2.5 hours prior to recording. Finally, α-DTX (100 nM), apamin (100 nM), and iberiotoxin (100 nM) were used to block K_v1.2-containing, SK, and BK channels, respectively. For experiments involving the application of K⁺ channel toxins, 0.005% bovine serum albumin (BSA) was included in both control and toxin-containing SIF solutions to minimize nonspecific binding.

Recordings were restricted to the lateral and anterior halves of the striatum, within ~500 μm of its dorsal border with the corpus callosum. Cells were visualized through a LUMPlanFI/IR 60X / 0.9 NA water-immersion objective (Olympus, Tokyo, Japan) using 590 nm LED illumination (Cairn Research Ltd., Faversham, Kent, UK) to identify tdTomato-expressing D1-SPNs and infrared Dodt Gradient Contrast illumination (Luigs & Neumann, Ratingen, Germany) to guide pipette placement. Patch pipettes were prepared from standard-wall, filamented borosilicate glass capillaries (BF150-86-10; Sutter Instrument Company, Novato, CA, USA) using a micropipette puller (P-97 Flaming/Brown; Sutter Instrument Company). Recordings were obtained using computer-controlled manipulators (Luigs & Neumann), a Multiclamp 700B amplifier, a Digidata 1440A digitizer, and pClamp 10 acquisition software (Molecular Devices, San Jose, CA, USA). Signals were low-pass filtered at 10 kHz online and sampled at 20–25 kHz. Cell and electrode capacitances were compensated electronically during recording, and voltage errors due to series resistance were manually corrected offline.

Optogenetic stimulation of ChR2(H134R)-expressing nigrostriatal DA axons was delivered via the microscope objective lens using wide-field 470 nm LED illumination (~2 mW/mm² under the objective; OptoLED; Cairn Research Ltd.). Individual stimulation pulse trains consisted of 5 or 20 light pulses (2 ms pulse duration) delivered at a frequency of 4 Hz or 20 Hz, as described in the main manuscript. For paired comparisons of the effects of 4 Hz and 20 Hz stimulation, stimulation order was balanced across the population such that an equal number of cells was recorded with 4 Hz or 20 Hz stimulation occurring first. The impact of single-pulse (2 ms) stimulation was evaluated in a separate cohort. In the majority of experiments, optogenetic stimulation was delivered as a train of 5 pulses at 20 Hz. When recordings employed repeated stimulation trials, each trial was separated by a minimum of 5 minutes to facilitate stable DA release across trials (Bass et al., 2013; Lu et al., 2015; Melchior et al., 2015).

Perforated-patch current-clamp recording

Perforated recordings were made using patch pipettes with an impedance of 4–6 MΩ when filled with the core internal solution, containing (in mM): 130 KMeSO₄, 10 NaCl, and 10 HEPES. The pH and osmolality of this solution were adjusted to 7.3 and 290 mOsm/kg, respectively. Patch pipettes were minimally front-filled with the core internal solution, and were then backfilled with the same solution containing gramicidin at a concentration of ~20 μg/mL. Gramicidin was used as the pore-forming agent for perforated recordings because gramicidin channels are selectively permeable to monovalent cations and small neutral molecules, but impermeable to chloride (Kyrzis and Reichling, 1995). Thus, gramicidin enables electrical access to recorded neurons without disrupting their anionic gradients, and is therefore less invasive than other methods of perforation. Alexa Fluor 594 Hydrazide (50 μM) was also included in the internal solution to provide visual feedback regarding the integrity of the membrane under the electrode: deliberate or accidental establishment of the whole-cell configuration (break-in) was indicated by rapid entry of the fluorescent dye into the soma of a recorded neuron. Alexa Fluor 594 fluorescence was monitored frequently throughout each experiment using 590 nm LED illumination (Cairn Research Ltd.), and recordings were discarded if break-in was detected. When a clean break-in was observed, the recorded membrane potential depolarized by an average of ~7 mV. This is slightly less than the estimated liquid junction potential of 8.7 mV between the internal and external solutions (Barry, 1994; Neher, 1992). The recorded membrane potentials were thus within 1–2 mV of the true membrane potential, and liquid junction potential corrections were not applied.

Perforated recordings were excluded only for the following technical reasons: (1) break-in occurred before the experiment could be completed; (2) stability of the recording was disrupted due to deterioration of the high-resistance seal between the patch pipette and the cell membrane; or (3) the recorded neuron failed to exhibit tdTomato fluorescence or characteristic electrophysiological properties of an SPN, as outlined in the Results section. Recordings were never excluded on the basis of their responsiveness to optogenetic stimulation. Series resistance values were determined offline for all perforated recordings that were used for comparison with whole-cell recordings (Figure 3) and/or for action potential waveform analyses (Figures 6–8 and S5). These values are reported in Tables S3 and S7–S10.

Whole-cell current-clamp recording

Whole-cell recordings were made using 4–6 MΩ patch pipettes containing (in mM): 130 KMeSO₄, 8.4 NaCl, 1 MgCl₂, 10 HEPES, 5 phosphocreatine, 0.1 Na₄-EGTA, 0.4 Na₃-GTP, and 2 Mg_{1.5}-ATP. To facilitate comparison with perforated recordings, this solution composition was chosen to match the Na⁺ and K⁺ equilibrium potentials (E_{Na} and E_K) in the perforated configuration. In addition, since gramicidin channels are not permeable to Cl⁻ and therefore do not affect E_{Cl} , E_{Cl} for whole-cell recordings was set at -67.5 mV to mimic the reversal of GABAergic postsynaptic potentials measured with gramicidin-based perforated recordings of SPNs (Bracci and Panzeri, 2006). The estimated liquid junction potential in the whole-cell configuration was 9 mV and was not corrected, meaning recorded whole-cell voltages were likely ~9 mV more depolarized than the true membrane potential. Whole-cell recordings were excluded only if the recorded neurons did not exhibit properties of D1-SPNs, or if the membrane seal quality was disrupted. Series resistance values were determined offline and are reported in Table S3.

Somatic current injection protocols

For the long up-state protocol, 1 s step current injections were delivered once per minute for 3–4 minutes to assess baseline excitability. Current levels were chosen based on minimum amplitudes required to elicit stable firing of at least 2 action potentials during the step (to enable calculation of instantaneous firing frequency): beginning with 100 pA, the injected current was gradually increased in 10–50 pA increments until these criteria were satisfied. The same current amplitude was then used for the long up state, which lasted for 10 s plus the duration of optogenetic stimulation (2 ms for single-pulse stimulation, 250 ms for 20 Hz stimulation, 1.25 s for 4 Hz stimulation). Regardless of frequency, optogenetic stimulation was always delivered in the middle of the long up state so that D1-SPN firing could be monitored for 5 s before and after. Current-only trials occurred one minute prior to optogenetic stimulation trials, and no adjustments to the current amplitude were made after the first optogenetic stimulation. Pre- and post-stimulus firing frequencies for this protocol represent the average instantaneous frequency during the 1 s immediately prior to optogenetic stimulation (pre) and during the last 1 s of the long current step (post). These pre- and post-stimulus time periods were extended to 2 s in length for the analysis of action potential threshold and AHP amplitudes. To monitor the persistence of modulation, responses to 1 s current steps were assessed once per minute for 10–20 minutes following optogenetic stimulation.

Each trial of the short up-state protocol consisted of 250 ms current steps delivered at a frequency of 1 Hz for a duration of 41 s. As for the long up-state protocol, optogenetic stimulation (20 Hz for 1 s) was delivered halfway through the trial. Pre- and post-stimulus measures reflect average responses during the first 20 or last 20 current steps in each trial, respectively. For this protocol, a single current-only trial was delivered prior to the first trial of optogenetic stimulation to determine the minimum amplitude of current that resulted in stable firing throughout the trial. Current amplitudes were not adjusted after this point, and no current was injected between trials. Each trial was separated by a period of 5 minutes, except after application of a new drug (e.g., SCH 23390 or isradipine), in which case 10 minutes were allowed for the compound to equilibrate before further testing.

Kir2 channel modulation was assessed using 250 ms subthreshold current steps eliciting ~5–10 mV depolarization from rest. Sub-threshold current steps were each followed by a 250 ms suprathreshold current step (start-to-start interval of 1 s) to assess dopaminergic modulation of firing frequency and latency. Pairs of sub- and suprathreshold current steps were delivered 5 s before and 1 s after optogenetic stimulation (20 Hz for 250 ms) of nigrostriatal DA axons. For this protocol, stimulation was delivered during the down state in order to (1) minimize voltage-dependent inactivation of Kir2 channels so that their positive or negative modulation by DA, if present, could be observed; and (2) examine whether dopaminergic modulation of firing properties would be altered under conditions of comparatively low intracellular Ca²⁺ levels.

Fast-scan cyclic voltammetry (FSCV)

Extracellular DA concentrations were measured using carbon fiber microelectrodes (CFMs) constructed according to published methods (Clark et al., 2010). Briefly, individual 7 μm-diameter carbon filaments (grade 34-700; Goodfellow Corporation, Coraopolis, PA, USA) were encased in 15-mm lengths of polyimide-coated fused silica capillary tubing (90 μm outer diameter; Polymicro Technologies, Phoenix, AZ, USA). The fused silica-carbon fiber junction was sealed at the tip with an inert, non-conductive epoxy. Exposed carbon fibers were trimmed to a length of ~50–100 μm. FSCV instrumentation and High Definition Cyclic Voltammetry (HDCV) Acquisition and Analysis software were provided by the Department of Chemistry Electronics Facility at the University of North Carolina, Chapel Hill (Bucher et al., 2013; <https://chem.unc.edu/critcl-main/critcl-electronics/critcl-electronics-hardware/>).

Brain slices were transferred to the recording chamber and continuously perfused with warmed, carbogenated SIF at a rate of 4–5 mL/min, as for electrophysiology experiments. Mecamylamine, scopolamine, Gabazine, CGP 55845, DNQX, and D-APV were included in the SIF for all FSCV experiments. FSCV detection of DA was accomplished by applying a triangular voltage waveform (-0.4 V to +1.3 V to -0.4 V at 400 V/s) to the CFM at a frequency of 10 Hz, while holding at a potential of -0.4 V (versus Ag/AgCl) between scans. The CFM tip was placed in the dorsolateral striatum 50–100 μm below the surface of the slice. Recording commenced after a stable background current was established with little to no drift and < 1–2 nA of noise over a period of 30 s. Optogenetic stimulation of DA release was patterned by a Master-8 pulse generator (A.M.P.I., Jerusalem, Israel) and offset from the CFM voltage scan by 10 ms to avoid photovoltaic artifacts. Optogenetic stimulation frequencies, pulse widths, and light intensities were identical to those used in electrophysiology experiments.

Extracellular DA signals were measured in 3 recording sites per slice, from 3 slices per animal. 3 patterns of optogenetic stimulation were applied at each recording site: single-pulse stimulation was always first, followed by 5 pulses at 4 Hz or 5 pulses at 20 Hz in balanced order. As for electrophysiology experiments, optogenetic stimulation trials were separated by a minimum of 5 minutes

to facilitate stable DA release. Data were analyzed using HDCV Analysis software (Bucher et al., 2013) after applying a fourth-order Bessel low-pass filter. Currents were measured at the peak oxidation potential for DA (~0.6 V versus Ag/AgCl). An average of 10 voltage scans occurring 500 ms before the onset of stimulation was used for background subtraction. Currents were then converted to DA concentrations as described below.

CFMs were calibrated to known concentrations of exogenous DA (0.25, 0.5, and 1 μ M dopamine hydrochloride freshly prepared in 50 μ M sodium metabisulfite) prior to first use as well as at the end of each experiment. Pre-calibration was necessary to determine the quality and sensitivity of each electrode, and selected CFMs were re-used as long as their response characteristics and post-experiment calibration values remained consistent and linear. Calibration factors for each CFM were determined through linear regression of average pre- and post-experiment responses to DA. The average calibration factor was 20.15 nA/ μ M DA (range = 14.02–23.81 nA/ μ M), with an average R^2 value of 0.98 (range = 0.96–1.0). All FSCV measurements exhibiting characteristic DA oxidation and reduction potentials (+0.6 V and –0.2 V versus Ag/AgCl, respectively) were included in the study. Data were excluded if CFM response characteristics deteriorated and the signal-to-noise ratio fell below acceptable limits.

Immunohistochemistry and confocal imaging

To optimize viral transfection and confirm the specificity of ChR2(H134R)-eYFP expression in nigrostriatal DA neurons, mice were deeply anesthetized with ketamine/xylazine (> 90/10 mg/kg, IP) in preparation for perfuse-fixation. Upon cessation of reflexes, mice were transcardially perfused at a rate of 1–2 mL per minute with 5–10 mL of 0.01 M phosphate-buffered saline (PBS, pH 7.4) followed by 30–60 mL of 4% paraformaldehyde (PFA) in 0.1 M phosphate buffer (PB, pH 7.4). Perfuse-fixed brains were then removed and post-fixed in 4% PFA (prepared in 0.1 M PB, pH 7.4) overnight at 4°C. Fixed tissue was washed with 0.1 M PB prior to the preparation of parasagittal sections (70 μ m) using a vibratome (VT1000 S; Leica Biosystems Inc.). Sections were then washed in PBS and processed for immunohistochemical detection of tyrosine hydroxylase (TH), a critical component of the catecholamine synthesis pathway that can be used as a marker of DA neurons in the brain regions investigated here. Free-floating sections were incubated for 48 hours at 4°C with mouse anti-TH primary antibody (1:5,000; MilliporeSigma, Burlington, MA, USA) in PBS supplemented with 2% normal donkey serum (NDS; Jackson ImmunoResearch Laboratories, Inc., West Grove, PA, USA) and 0.5% Triton X-100 (MilliporeSigma). After washing in PBS, sections were then incubated for 90 minutes at room temperature with Alexa Fluor 594- or Alexa Fluor 647-conjugated donkey anti-mouse IgG (1:250; Jackson ImmunoResearch Laboratories, Inc.) in PBS containing 2% NDS and 0.5% Triton X-100. Following a final wash in PBS, slices were mounted on glass slides using ProLong Diamond antifade mountant (Thermo Fisher Scientific, Waltham, MA, USA), coverslipped, and cured at room temperature for a minimum of 24 hours prior to imaging.

ChR2(H134R)-eYFP, tdTomato, and immunohistochemical labeling for TH were visualized using either epifluorescence microscopy (Axioskop 2; Carl Zeiss) or confocal laser scanning microscopy (A1R or A1; Nikon Instruments Inc., Melville, NY, USA). Epifluorescence microscopy was used to monitor viral transfection and optimize the injected titer for each new lot of AAV9.EF1a.DIO.hChR2(H134R)-eYFP.WPRE.hGH (Penn Vector Core). Images of TH immunoreactivity and ChR2(H134R)-eYFP labeling in substantia nigra pars compacta (SNC) cell bodies (Figure 1B) were acquired using a Plan Apo Lambda 60X, 1.4 NA oil-immersion lens on a Nikon A1R confocal microscope. Images of TH immunoreactivity and ChR2(H134R)-eYFP expression in nigrostriatal axons along with D1-SPN tdTomato expression in the dorsolateral striatum (Figure 1C) were acquired using a Plan Apo 20X, 0.75 NA objective on a Nikon A1 confocal microscope.

QUANTIFICATION AND STATISTICAL ANALYSIS

Only data that were compromised for technical reasons, as specifically outlined above, were excluded. Confocal images shown in Figures 1B and 1C were stacked and adjusted for brightness and contrast using Fiji (Schindelin et al., 2012). Image pseudocoloring was then adjusted using Photoshop (Adobe, San Jose, CA, USA). FSCV data were initially processed using HDCV Analysis software (Bucher et al., 2013). The decay of each evoked DA transient (truncated at 5 s following the peak response at the end of optogenetic stimulation; Figures 1F and S1C) was well fit with a monoexponential function (ExpDec1) in Origin 2016 (OriginLab Corporation, MA, USA). Electrophysiological data were analyzed using Clampfit 10.7 (Molecular Devices) and Origin 2016 (OriginLab Corporation). Subthreshold responses to current injection shown in Figure 5A (expanded zoom only) were filtered offline using a 2.5 kHz FFT low-pass filter, for visualization purposes only. Action potential threshold values (Figures 6A, 6B, 7A, 7B, 8G–8J, S5F, and S5G) were calculated from waveform averages by determining the first point of sustained positive acceleration (second derivative) of voltage that exceeded 2 SD of the acceleration “noise” 5–10 ms prior to threshold. Measurements of action potential half-width, maximum rate of rise, and maximum rate of decay from the long up-state protocol (Figures S5A–S5D), as well as all action potential properties from the short up-state protocol (Figures S5F–S5M) were taken from waveform averages representing 2 or 20 s per condition for long and short up-state data, respectively. Except for experiments in which SK and BK channel toxins were applied, AHP voltages (Figures 6C–6H, 7C–7F, and 8M–8O) were measured individually from raw traces prior to averaging. Fast- and medium-duration AHPs were not easily distinguished in the presence of apamin and iberiotoxin (Ap/IbTX); therefore, AHPs (Figures 8P–8R) were measured from waveform averages, with Ap/IbTX values representing voltages at equivalent time points to their respective control AHPs.

Given the relatively small sample sizes used in the majority of this study, a normal distribution of the data could not be reliably tested or assumed (Wilcox and Rousselet, 2018). Therefore, two-tailed, non-parametric statistical comparisons were made using the Wilcoxon signed-rank (WSR) test for paired data or the Mann-Whitney U (MWU) test for unpaired data. Correlated changes in action potential threshold and AHP amplitudes (Figures 7F, 8O, 8R, S5E, and S5M) were evaluated using two-tailed, non-parametric Spearman correlations and are represented by the rank correlation coefficient, ρ . Statistics were calculated using Prism 8 software (GraphPad Software, San Diego, CA, USA); $p < 0.05$ was considered significant. Tilted line segment plots in each figure represent paired observations, and superimposed box plots illustrate the median (central line), interquartile range (box) and 10%–90% range (whiskers) of each condition or group. Summary statistics (median and interquartile range), associated numbers of cells and mice, and p values for each statistical comparison are shown for all datasets in Tables S1–S10. The Holm-Bonferroni method (Holm, 1979) was used to correct for multiple comparisons in Figures 1E, 1F, 2F (also shown in S2B), 2H (also shown in S2D), 4D, and 4E. Both raw and corrected p values are presented for these data in Tables S1, S2, and S4. Families of comparisons were defined as those relating to a singular hypothesis, tested on the same group of neurons by multiple means. For example, Figure 4D (and likewise, 4E) presents 2 comparisons each addressing distinct hypotheses concerning acute dopaminergic modulation, persistent dopaminergic modulation, and progressive occlusion of effect size; associated p values were thus corrected for 2 comparisons per hypothesis. Asterisks within Figures 1E, 1F, 2F (also S2B), 2H (also S2D), 4D, and 4E indicate $p < 0.05$ before and after correcting for multiple comparisons. Asterisks surrounded by parentheses in Figure 2F (also S2B) represent $p < 0.05$ before, but not after, correcting for multiple comparisons.

DATA AND CODE AVAILABILITY

All datasets contributing to this study are summarized in Tables S1–S10, as described above. Raw and analyzed data from each individual experiment have also been deposited on the Open Science Framework and are available at <https://doi.org/10.17605/OSF.IO/QUW5J>.